This manuscript is a preprint uploaded to EarthArXiv. This preprint has been submitted to Journal of Hydrology for peer review. Subsequent versions of this manuscript may have slightly different content. We welcome feedback, discussion, and comments at any time. Feel free to contact the authors.

Spatiotemporal Variation in Cave Percolation Waters: A Functional Approach

Rebecca G. Chapman[1*], Shawn Laffan[1], Liza K. McDonough[2], Monika Markowska[3], Andy Baker[1]

[1] School of Biological, Earth and Environmental Sciences, UNSW Sydney, NSW, 2052, Australia

[2] Australian Nuclear Science and Technology Organisation (ANSTO), New Illawarra Rd, Lucas Heights, NSW, 2234, Australia

[3] Climate Geochemistry Department, Max Planck Institute for Chemistry, Mainz, 55128, Germany

*Corresponding author: rebecca.chapman@unswalumni.com

Abstract

Understanding the mechanisms controlling spatial heterogeneity of drip water percolation into caves is essential for interpreting karst aquifer recharge and speleothem isotopic and geochemical records for paleoclimate analyses. Here we present the first analysis of drip rate variability using a novel time-varying Functional Principal Component Analysis (FPCA), validated against drip water stable isotope composition. Twenty-six drip sites were monitored across Harrie Wood Cave, south-east Australia, over a 2.5 year period. A positive relationship with cave drip water hydrology and rainfall and soil moisture was identified, with soil moisture recording the strongest relationship. FPCA was used to classify drip-water flow (percolation) pathways based on temporal shifts in the drip rate time series. Our results reveal that three percolation classes can be used to explain water movement within the cave: storage baseflow, fracture baseflow and overflow. The successful application of FPCA in this study suggests that this statistical technique will be useful for the analysis and interpretation of other large, discontinuous hydrological datasets.

Keywords: time-series, FPCA, percolation classes, spatial analysis

1. Introduction

Karst regions represent 15.2% of the Earth's land surface (Goldscheider et al., 2020) and play a key role in society and the environment. Karst regions have the ability to store water, operate as a carbon sink, and promote biodiversity (Clements et al., 2006; Goldscheider, 2019; Hartmann et al., 2009; Kempe, 1979). Approximately 9.2% of the global population relies upon karst aquifers for water use (Stevanović, 2019), with an estimated 1.3 billion people living in karst regions (Goldscheider et al., 2020). These regions, however, are increasingly being impacted by human activity (Lukač Reberski & Terzić, 2022), highlighting the importance of understanding karst recharge processes so that relevant management plans can be implemented.

The dissolution of karst in the subsurface results in selective pathways, as water flows preferentially towards fractures, often following geological features such as bedding planes (Ford and Williams, 2013). Over time, further conduits, fractures, and fissures form, with some widening enough to form caves (Ford, 2007). These karstic features tend to be more prevalent in the upper subsurface zone (the epikarst), a region subject to greater weathering and thus increased fracturing (Williams, 1983). The relationship between rainfall and karst recharge is typically non-linear, and in some areas water percolation through the epikarst is indirect, and most likely held in epikarst storage reservoirs for variable time periods (Baker and Brunsdon, 2003; Partin et al., 2012). These epikarst water storage reservoirs can drain through the unsaturated zone via a combination of matrix, fracture and conduit flows, depending on the characteristics of the karst geology. Water flow through the epikarst is difficult to model due to the heterogenous nature of flow paths, in the unsaturated zone, which in turn leads to non-uniform percolation rates (Arbel et al., 2010; Jex et al., 2012; Markowska et al., 2015; Poulain et al., 2018; Sheffer et al., 2011). Cave drip rates, however, can provide valuable insight into the functioning of the epikarst and wider karst unsaturated zone, and assist in determining rainfall recharge thresholds and unsaturated zone storage capacity (Baker et al., 2021).

Traditional statistical methods are typically applied to drip water hydrology time series to characterise drip percolation type. Multi-dimensional scaling (MDS), traditional Principal Component Analysis (PCA), Agglomerative Hierarchical Clustering (AHC) and k-means clustering have been used with time series derived from spatially dense networks of loggers to identify similarities between drip sites and clusters respectively (Jex et al., 2012; Mahmud et al., 2018, Markowska et al., 2015). These conventional statistical cave drip water classification techniques can be problematic for time series data, however, as they analyse the discrete values in the drip water timeseries rather than considering the entire shape of the hydrograph. As a result, they may potentially miss underlying functional behaviour. Furthermore, traditional statistics tend not to take autocorrelation into account when calculating degrees of freedom, leading to an overestimation of significance in variation (Hassani et al., 2012). These issues can be overcome using Functional Data Analysis (FDA) techniques which express a series of discrete measurements as a function, for example, of time (Wang et al., 2016). The advantages of FDA include: (1) it does not require uniformly sampled data, (2) is not subject to parametric assumptions, and (3) it reduces noise across the data (Ramsay and Silverman, 2005). Furthermore, issues of autocorrelation are minimised due to the discrete values of a timeseries being considered as a single entity (Ullah and Finch, 2013).

Markowska et al. (2015) utilised cross-correlation analyses to determine the relationship between drip water hydrology, precipitation and soil moisture. To compare, this study also applies cross-correlation analyses to the drip rate time series. Markowska et al. (2015) previously used traditional PCA and AHC techniques to isolate variability and assess similarities in a one-year drip hydrology time series from Harrie Wood Cave (current study) to classify the flow types of fourteen drip water sites. Our study builds on this research by applying Functional Principal Component Analysis (FPCA) to a larger drip rate time series dataset over a longer monitoring period to assess variability in drip rate with time. FPCA results combined with cross-correlation analyses and drip water stable isotope composition are used to characterise drip sites into percolation classes. In doing this we aim to 1) identify temporal variability in drip water dynamics to elucidate how water percolates from the surface to the cave, 2) establish drip rate response to hydrological inputs (precipitation and soil moisture) and, 3) analyse spatial patterns in drip rate variability and stable isotope values to conceptualise cave water percolation processes. Drip water stable isotope data are also assessed for a more robust classification of drip flow type (Campbell et al., 2017), since isotopic variability can be used to determine whether statistical percolation classification is logical (Fairchild and Baker 2012).

1. Materials and Methods

2.1. Region and Site Description

The study site is Harrie Wood Cave, located within the Yarrangobilly karst area, Snowy Mountains, New South Wales, Australia (Figure 1).

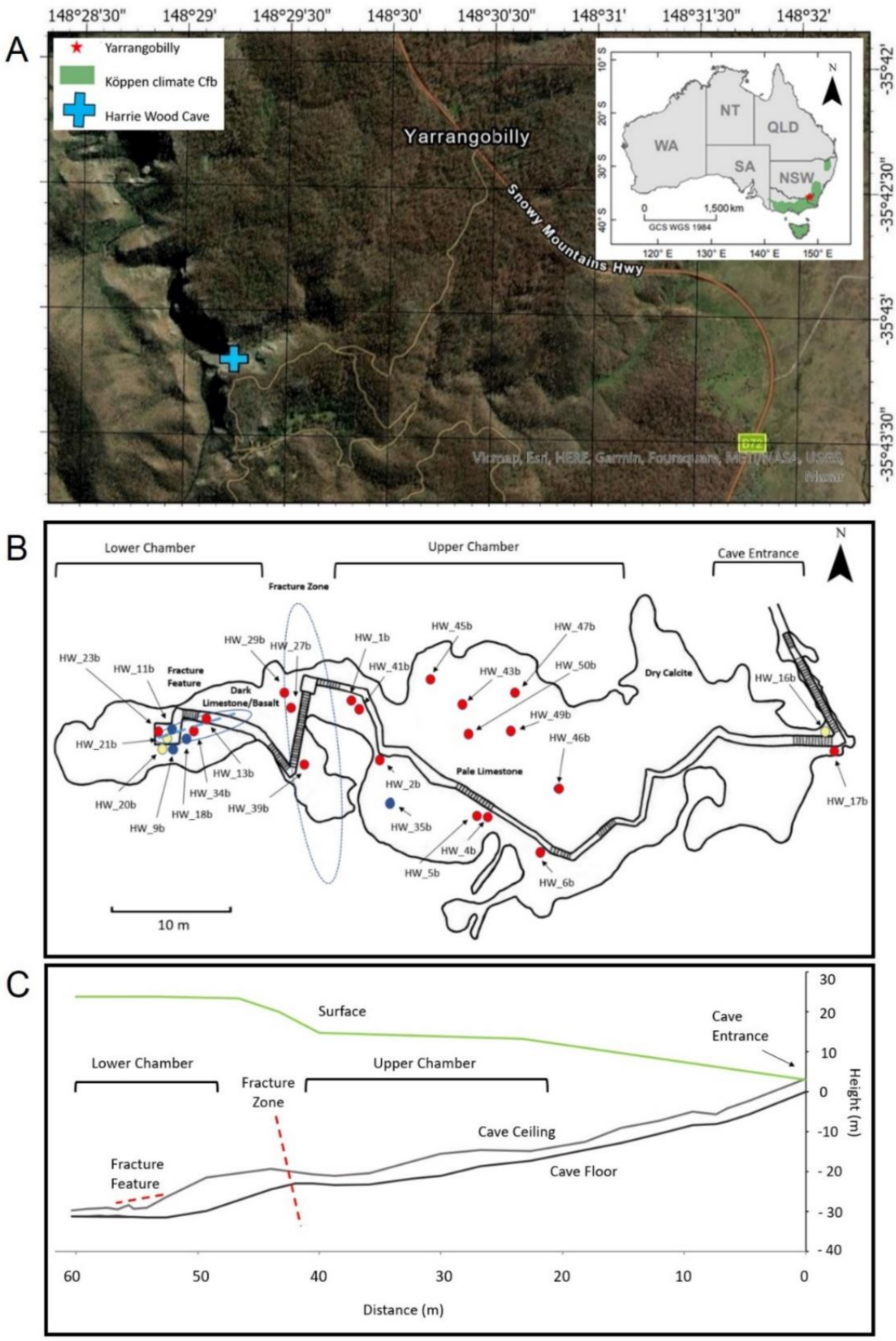

Figure 1: (A) The location of Yarrangobilly and Harrie Wood Cave in New South Wales, adapted from Coleborn et al. (2016). Yarrangobilly is in the south-east Australian Region classified as temperate oceanic climate or subtropical highland climate (Cfb) as per the Köppen Climate Classification (Peel et al., 2007) (B) Drip logger sites used in analysis across Harrie Wood Cave, with cave outline adapted from Nicholl (1974). Drip loggers are indicated by circles, with red sites corresponding to storage baseflow, blue sites corresponding to overflow and

yellow sites corresponding to fracture flow. Drip site classes are explained in section. 4.1.2 and Figure 8 (C) Depth Profile of Harrie Wood Cave adapted from Markowska et al. (2015).

The region is in a montane temperate environment with dry summers, with an average temperature of 17° C and wet winters, including snowfall, with an average temperature of 5.5°C (Bureau of Meteorology, 2022). Annual precipitation (1276 mm/a) in the region is impacted by climate drivers including the El Niño Southern Oscillation (ENSO) (Tadros et al., 2019, 2016) and the Indian Ocean Dipole (IOD) (Risbey et al., 2009; Scroxton et al., 2021). Due to the steepness of the local terrain, vegetation is sparse and shrubby and shallow soil covers the surface, with intermittent limestone outcroppings (Figure S1). Notably, the state of vegetation and soil during the study period may have been impacted by the 2019/2020 Black Summer Bushfires that burnt across the site.

The Yarrangobilly karstic belt formed in the Late Silurian from coral deposits with karstification occurring along NE/SW faults (Worbys, 1982). Speleogenesis began in the Pleistocene (Brush, 2016), resulting in highly marbleised and fractured limestone with low porosity (Spate, 2016), typical of Eastern Australian limestone. Harrie Wood Cave is located on a steep, northwest facing slope of massive limestone (Figure 1). It was likely developed through phreatic and vadose processes, with the exposed basalt boulders and gravel in the lower chamber providing evidence of remnant fluvial deposits (Figure S2) (Brush, 2016; Spate, 2016).

The cave entrance is at 915 m altitude and follows westwards decline to descend 30 m into the unsaturated zone, with overburden varying from ~30 m to ~60 m. The cave consists of two distinct chambers: the upper chamber (~ 20 m x 18 m) and the lower chamber (~ 10 m x 5 m). The two chambers are separated by a fracture zone, characterised by the shift of pale limestone to darker limestone (Markowska et al., 2015). The upper chamber slopes southwards and is adorned with larger stalagmites and massive columns (Figure S3). Observations during a site visit in September 2022 identified a hydrological gradient with the upper (northern) reaches characterised by dry calcite, to small pools and puddles forming in the lower (southern) reaches. The lower chamber is characterised by a fracture feature, split by draperies and cave popcorn (Figure S3). Speleothems (cave mineral deposits) in the lower chamber are observed to be smaller and exhibited signs of active growth fed by constant drip water in September 2022.

2.2. Hydrological, soil, climatic and spatial data

2.2.1. Hydrological Data

Drip percolation in Harrie Wood Cave has been extensively monitored by up to 52 Stalagmate ® Plus Mk2b acoustic drip loggers since 2011, sampling at an interval of 15 minutes. Twenty-six of these loggers were used in this study (Figure 2B). The naming convention for these loggers is “HW_nb” where HW denotes Harrie Wood, “n” is the site number and “b” indicates the logger was installed after 2011 (e.g. HW_9b). Drip data were aggregated to daily intervals to minimise noise (Mahmud et al., 2018). The period selected for analysis was July 2014 – January 2017 as it had the highest number of active drip loggers. Drip sites with >20% missing data from the study period were excluded from analysis. Eight of the sites analysed by Markowska et al. (2015) were also used in this study.

Variations in drip water $\delta^{18}O$ can be used to trace hydrological conditions. In general, south-eastern Australian drip water stable isotopes are controlled by a combination of an ‘amount effect’ during high-volume precipitation events. This leads to more negative value during wetter conditions and an evaporative effect of fractionation of vadose water during drier periods, resulting in more positive values (Cuthbert et al., 2014, Tadros et al., 2022). Drip water $\delta^{18}O$ can also provide an indication of flow path type, for example Treble et al. (2022) identified that drip waters transported via matrix flow displayed more positive $\delta^{18}O$ than those transported via fracture flow paths.

Drip waters were sampled over 6 sample campaigns across sites in Figure 1B and collected in 7 ml glass exetainer vials with no headspace. Samples were analysed at ANSTO on a Picarro Cavity Ring-Down Spectrometer (reported accuracy of ±0.15‰ for $\delta^{18}O$). The $\delta^{18}O$ values were normalised to in-house calibration standards, standardised to VSMOW2 and SLAP and reported in per mille (Tadros et al., 2022). The spot-sampling campaigns varied in spatial density (Table S1) and resulted in inconsistent monitoring intervals for some sites and therefore these are used as supporting data.

2.2.2. Precipitation and Soil Moisture Data

Daily rainfall measurements (Figure 2A) were sourced from the Yarrangobilly Caves weather station (Bureau of Meterology, 2022), ~ 750 m from the study location. Soil moisture saturation was measured at an interval of fifteen minutes by a Stevens Hydra Probe ® situated above Harrie Wood Cave at a depth of 25-30 cm (Markowska et al., 2015;Tadros et al., 2019). The soil moisture data was aggregated to daily intervals (Figure 2B) for consistency with the aggregated drip logger data.

2.2.3. Spatial Data

Cartesian coordinates obtained from a complete cave survey outlined in Markowska et al. (2015) were georeferenced to GDA2020 using a first order polynomial transformation (Figure 4).

2.3. Statistical Methods

All statistical analyses were undertaken using RStudio version 2022.02.1. Further details are provided below.

2.3.1. Cross-correlation

Precipitation and soil moisture measurements were selected as variables representative of hydrological inputs to Harrie Wood Cave (Markowska et al., 2015; Tadros et al., 2016). Missing data can cause a bias in cross-correlation analyses, therefore time periods with missing drip values were omitted from analysis. Autocorrelation for each variable was estimated using the `acf()` function from the `stats` package (R Core Team, 2022). Cross-correlation determines the degree of similarity between two timeseries and is useful in recognising temporal lags between variables. Therefore, cross-correlation analysis, using the `ccf()` function from the `stats` package (R Core Team, 2022) was used to understand (1) whether drip rates had a significant response to antecedent rainfall or soil moisture conditions, and (2) at what lag was there significant response (Markowska et al., 2015; Tagne and Dowling, 2018).

The lag timestep was set to daily with the maximum lag defined as 21 days, based on existing hydrological recharge thresholds in neighbouring caves (Baker et al., 2021). The minimum lag was set to zero days.

2.3.2. Functional Decomposition of Drip Data

FPCA is an FDA method that analyses functions instead of observations, capturing temporal structure to reduce the effects of temporal autocorrelation (Zhou and Müller, 2022). It is still a relatively novel technique for the analysis of longitudinal time series analysis, with hydrological studies so far only using FDA techniques on stream discharge and streamflow data (Ternynck et al., 2016). For FPCA analyses, our data was first log transformed ($\log_{10} +1$) to reduce extremes in magnitude. Generalised peaks are retained to signal prolonged hydrological events, however the focus is on the underlying functional behaviour. Across the data, significant gaps were recorded with 46% of days logging at least one drip site with no values. Therefore a Principal Analysis by Conditional Expectation (PACE) algorithm was applied using the `fdapace` package (Gajardo A et al., 2021) in R (R Core Team, 2022) to estimate functional principal components (FPC's) though best linear predictors in lieu of missing data. The steps for FPCA and the PACE method and relevant equations are explained in Chen et al. (2017) and Wang et al. (2016).

FPCA was undertaken with a smoothing bandwidth of 22.85 (2.5% of observations in drip rate timeseries) for the mean and 45.7 (5% of observations in drip rate timeseries) for the covariance. Smoothing bandwidths of 5% for mean and 10% for covariance were experimented with and had no meaningful effect on results. Relative FPCA scores and trajectories of curve behaviour were used to indicate the main driver of flow and classify drip sites into three categories of storage baseflow and fracture flow (or overflow) per Friedrich & Smart (1982) , and an additional overflow classification.

3. Results

Here we present the results, beginning with the hydroclimatic and isotopic data, followed by the cross-correlation results which compare the correlation between drip rates, soil moisture and rainfall. This is used to determine connectivity (rate and extent, including lags, in transmission of water) between the land surface and the cave environment. Spatial heterogeneity of drip water stable isotope ($\delta^{18}O$) values are presented and examined in relation to water storage and flow paths throughout the cave. FPCA results are then presented to describe the major trends in drip rates over time which are used to determine flow path classification at each site (fracture flow, overflow and storage baseflow).

3.1. Hydroclimate: 2014 – 2017

The time series results for the monitoring period are presented in Figure 2. The monitoring period encompasses a drier than average year in 2015 (993.1 mm), influenced by a weak El Niño and a wetter than average year in 2016 (1551.6 mm), influenced by a strong negative Indian Ocean Dipole (IOD) (Bureau of Meterology, 2022). By monitoring a wet and dry year, the risk of bias towards specific climatic conditions when interpreting results is minimised. Figure 2A shows an increase in precipitation frequency which corresponds with persistent higher levels of soil water content and increased percolation of water throughout the cave. The cooler months (April – September) correspond with increased hydrological activity of the percolation waters throughout the cave, with 2016 demonstrating a longer sustained period of percolation than 2015, indicating a response to climatic conditions. The general behaviour of cave percolation appears to align with rainfall events, potentially driving the flashy nature of the hydrology of certain drip water sites, with soil moisture providing a more consistent moisture source. These relationships were quantified using cross-correlation.

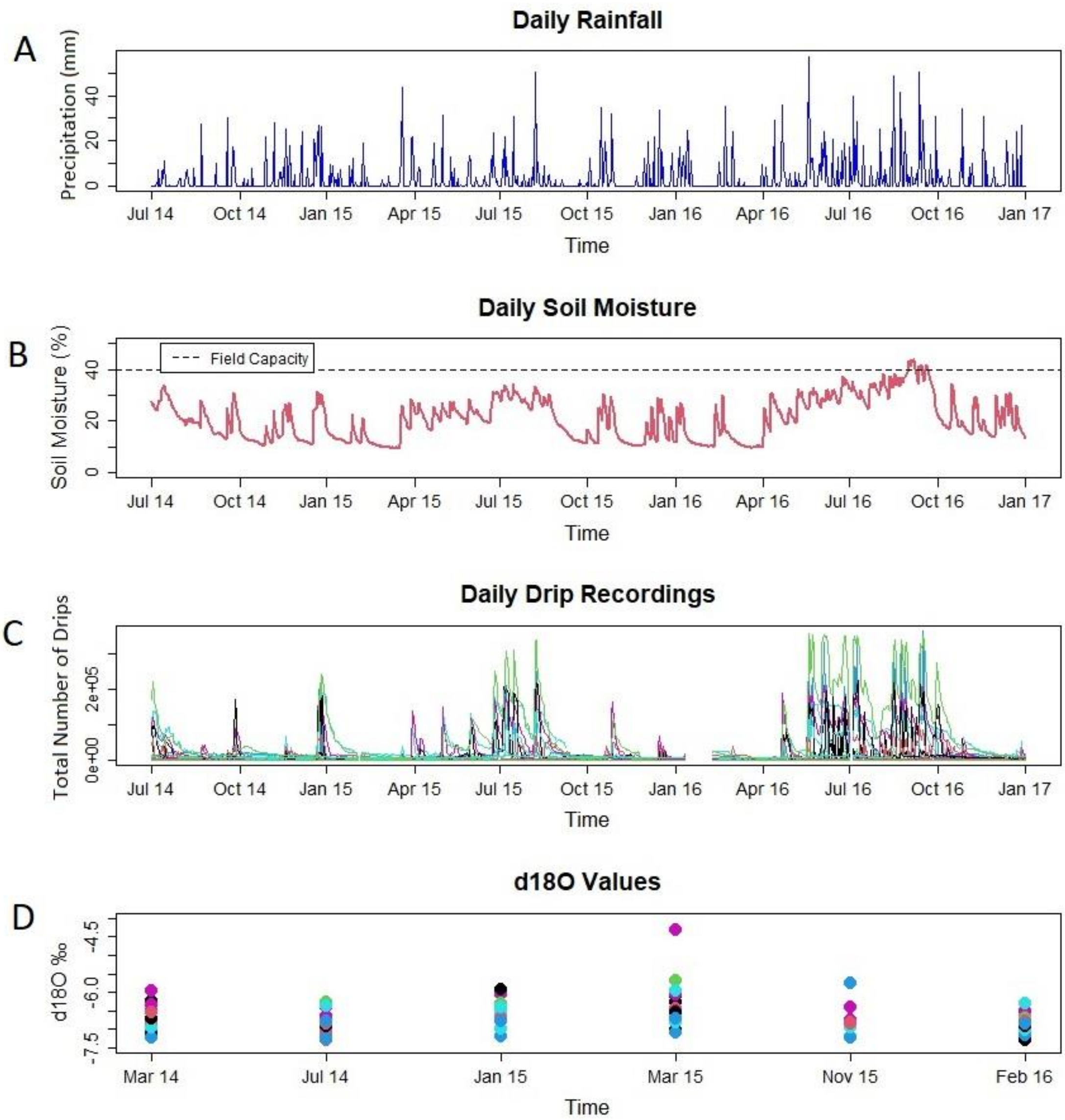

Figure 2: (A) Daily precipitation measurements from Yarrangobilly Caves Station (Bureau of Meterology, 2022). (B) Daily soil moisture measurements from a soil sensor above Harrie Wood Cave with the saturation field capacity highlighted at 40% (Tadros et al., 2019). (C) Daily drip recordings from twenty-six loggers for the monitoring period. Each colour represents a different site indicating the variation in magnitude and frequency of drips. (D) $\delta^{18}O$ values from drip water at each site across six spot sampling campaigns from 2014-2016. A relatively constant spread of values is reported across seasons. All $\delta^{18}O$ values are reported in VSMOW2, with the precipitation weighted mean (PWM) for Harrie Wood Cave as -7.0 ‰ (Tadros et al., 2022).

3.2. Cross-Correlation Analysis

3.2.1. Precipitation

Precipitation and soil moisture were identified as the leading variables respectively and drip rate were identified as the lagging variable, with each drip water percolation site analysed separately. Precipitation displayed a significant autocorrelation for a lag of 2 days, indicating that cross-correlation results beyond this scope are not skewed by internal data autocorrelation.

Cross-correlation plots were generated for each drip site against precipitation and soil moisture data, respectively (Figure S4, Figure S5) displaying the correlation value at shifting daily lags. A positive correlation was recorded for all sites for both parameters except HW_18b (Figure S4), which recorded a weak negative relationship indicating karst controls dominate drip rate at this site more strongly than precipitation and soil moisture. Across all sites there was a relatively low correlation of drip water percolation rate to precipitation with the highest coefficients ranging from 0.115 (HW_4b) to 0.528 (HW_23b) and with a lag between zero to four days (Figure S4). The shape of the curve on the cross-correlation plots gave a stronger indication of the true response to precipitation (Figure S4). For example, precipitation cross-correlation plots with a rapidly decaying structure from zero to one days, indicate a short rapid percolation period in correlation to a precipitation event. Sites HW_1b, HW_4b, HW_20b, HW_21b, HW_47b (Figure S4) display this correlation plot type along with a relatively high correlation coefficient indicating these sites are more likely to be linked to fractures ensuring relative connectivity to the surface. Plots with a relatively flat curve and small peak indicate weaker correlation with precipitation. This is likely representative of a steady baseflow or overflow as the epikarst reservoir has drained over time with examples including HW_35b and HW_13b (Figure S4).

In a spatial context, loggers with a lower correlation with precipitation were recorded exclusively on the western side of the fracture feature in the lower chamber (Figure 3A). This could be a result of increasing depth, or that the fracture feature is diverting flow.

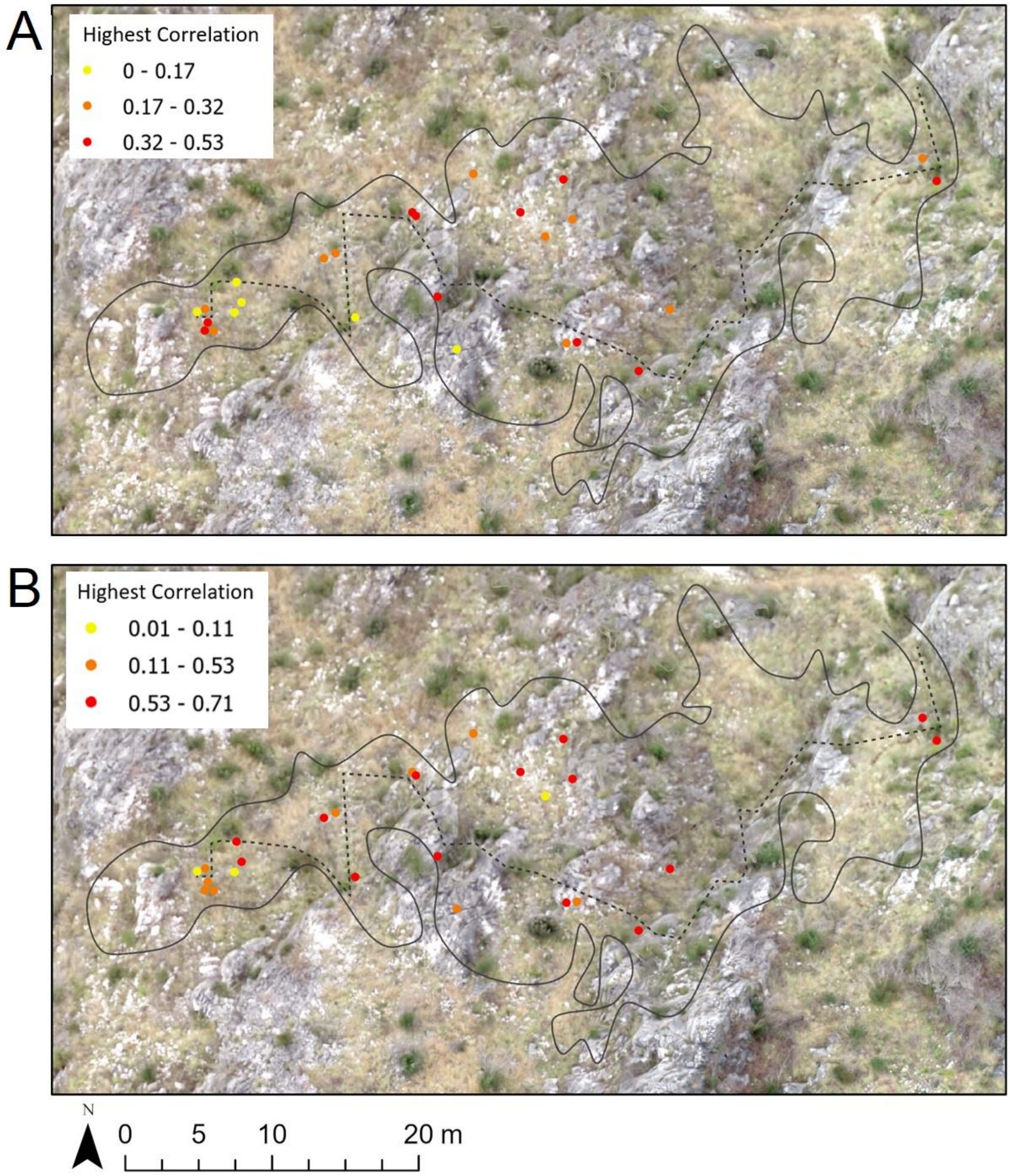

Figure 3: (A) Spatial distribution of highest precipitation cross-correlation coefficient recorded for each drip site. A general weakening in relationship with increasing depth is observed. Three classes were assigned using Jenks natural breaks. (B) Spatial distribution of highest soil moisture correlation-coefficient for each drip site, exhibiting spatial heterogeneity.

3.2.2. Soil Moisture

Soil moisture showed significant autocorrelation for a lag of 95 days, approximately the length of a season, indicating a seasonal driving mechanism of soil moisture function. The cross-correlation outputs reflected this autocorrelation as most sites took more than two months to drop below the 0.05 confidence interval (Figure S5). Soil moisture recorded stronger cross-correlations to drip rate than did precipitation, with highest correlations ranging from 0.714 (HW_6b) to 0.114 (HW_18b) (Figure S5). HW_6b also recorded the strongest relationship with soil. This is consistent with Markowska et al. (2015) and indicates this site likely has high connectivity to the soil storage reservoir.

All sites except HW_50b displayed a positive correlation at the initial time of increased drip rates (where “Lag (Days)” is equal to zero on the x-axis, Figure S5). Drip sites with a relatively low correlation that maintain a relatively flat curve, such as HW_11b (Figure S5), likely have an indirect and limited relationship with soil moisture inputs. Notably, fifteen of the drip sites recorded a secondary peak between days 10-18, with thirteen sites displaying the strongest correlation at a lag of 11-12 days (Figure S5). This delay indicates a temporal constraint to a potential drainage of the soil storage reservoir, where it may take just under two weeks for soil derived water to reach the drip sites. This phenomenon did not appear to follow a depth transect, with sites HW_17b (entrance), HW_41b (upper chamber) and HW_13b (lower chamber) all exhibiting dual peak behaviour with relatively high correlation coefficents (Figure S5).

The extent of correlation diminishes with depth, with both drip sites at the entrance exhibiting high correlation and the lower chamber recording a lower correlation on average

(Figure 3B). However, the spatial pattern for this is relatively weak (Figure 3B), indicating that there is not a simple depth relationship between soil moisture saturation and drip rate.

3.3. Drip Water Stable Isotope Variability

Variations in drip water $\delta^{18}O$ values from each site (Figure 2D) reflect spatial heterogeneity in $\delta^{18}O$ values in the cave at any given time. The variability of $\delta^{18}O$ is most likely due to varying retention of water in the epikarst based on the different drip water percolation paths, leading to mixing of drip water (Callow et al., 2014; Tadros et al., 2016).

The weighted mean of precipitation for Harrie Wood Cave is -7.0 ‰ (Tadros et al., 2022), which is lower than the mean drip water $\delta^{18}O$ recorded over the monitored period presented in this study (2014-2016) (Figure 4A). A spatial pattern emerged where sites with more negative $\delta^{18}O$ were located close to the fracture zone between the two chambers, indicating that the fracture was altering flow (Figure 4A). Furthermore, drip sites experiencing the greatest variation of $\delta^{18}O$ values were predominantly in the lower chamber (Figure 4B), with two highly variable sites recorded in the upper chamber. The two entrance sites recorded little variation and consistently recorded ~-7.0 ‰. A split in isotopic behaviour on either side of the fracture zone was apparent (Figure 4A), inferring the occurrence of two epikarst storage reservoirs.

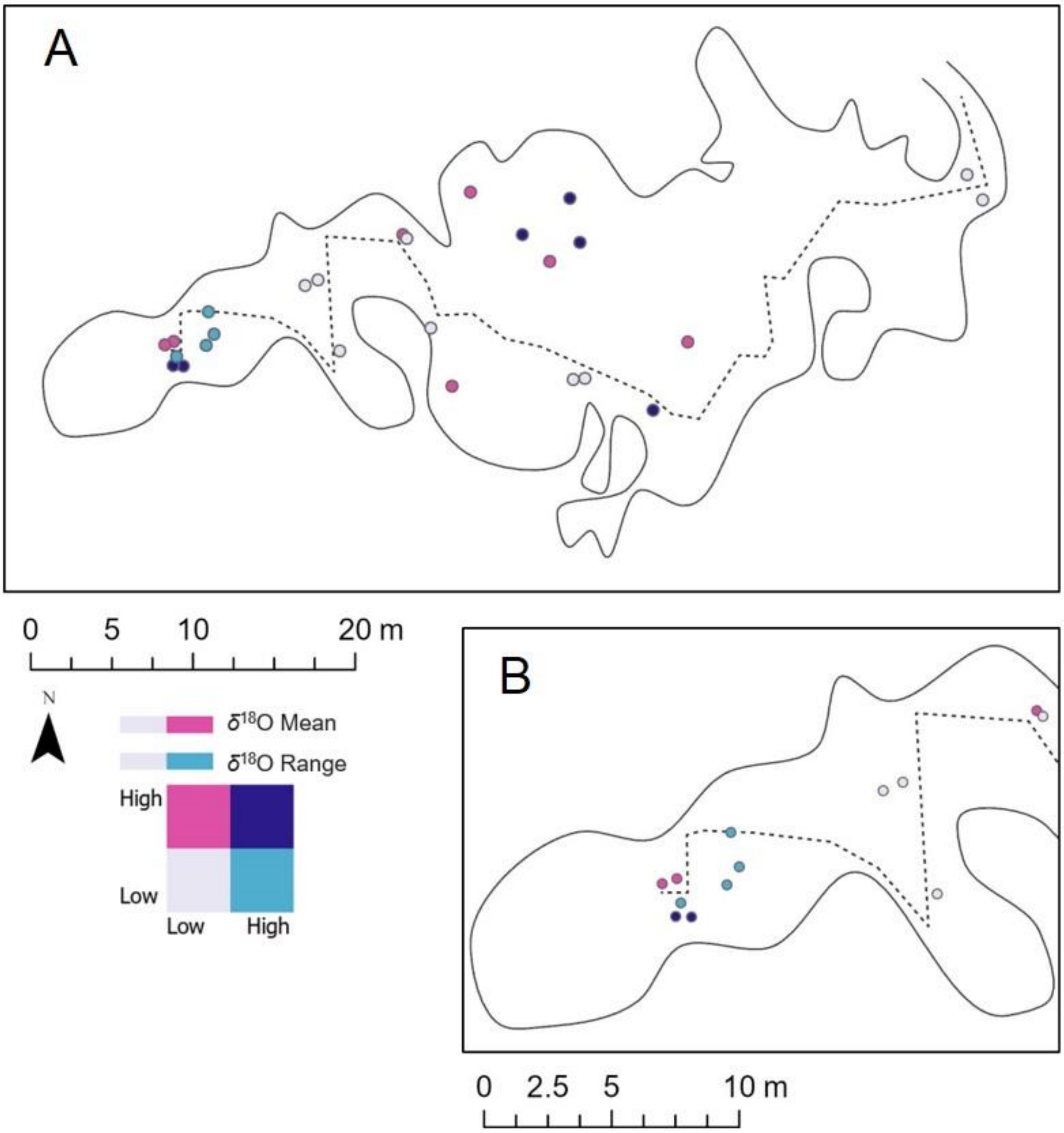

Figure 4: (A) Spatial distribution of mean and range of $\delta^{18}O$ values recorded for each drip site, sampled across 2014 - 2016. (B) Same data but zoomed to the lower chamber. The lower chamber records a greater concentration of highly variable isotopic signatures at respective sites than the upper chamber. Points coloured in dark blue represent sites where the mean and range of drip water $\delta^{18}O$ are high (mean ≥ -6.784, range ≥ 0.61). Points coloured in pale pink represent sites where the mean and range of drip water $\delta^{18}O$ are low (mean < -6.784, range < 0.61). Points coloured in pink represent sites where the drip water $\delta^{18}O$ mean is high and the drip water $\delta^{18}O$ range is low and light blue points represent the sites with drip water $\delta^{18}O$ values with a low mean and high range.

3.4. FPCA

3.4.1. FPC Scores

The estimated FPC scores for each drip site explain alignment to respective eigenfunctions (Yao et al., 2005). The FPC scores can be used to understand which mode of variation is driving drip behaviour to identify which drip rate time series are exhibiting similar functional behaviour. Drip site specific FPC scores are summarised in Figure 6. A large score indicates alignment with the respective eigenfunction, with a positive or negative score interpreted as directional alignment in time (Chen et al., 2017). Drip sites shown in Figure 5 including sites 20, 21, 11, 18, 9,16 and 35 (i.e., HW_20b, HW_21b, HW_11b, HW_18b, HW_9b, HW_16b and HW_35b, respectively) were observed to display different drip behaviour to the majority of the drip sites and are considered outliers.

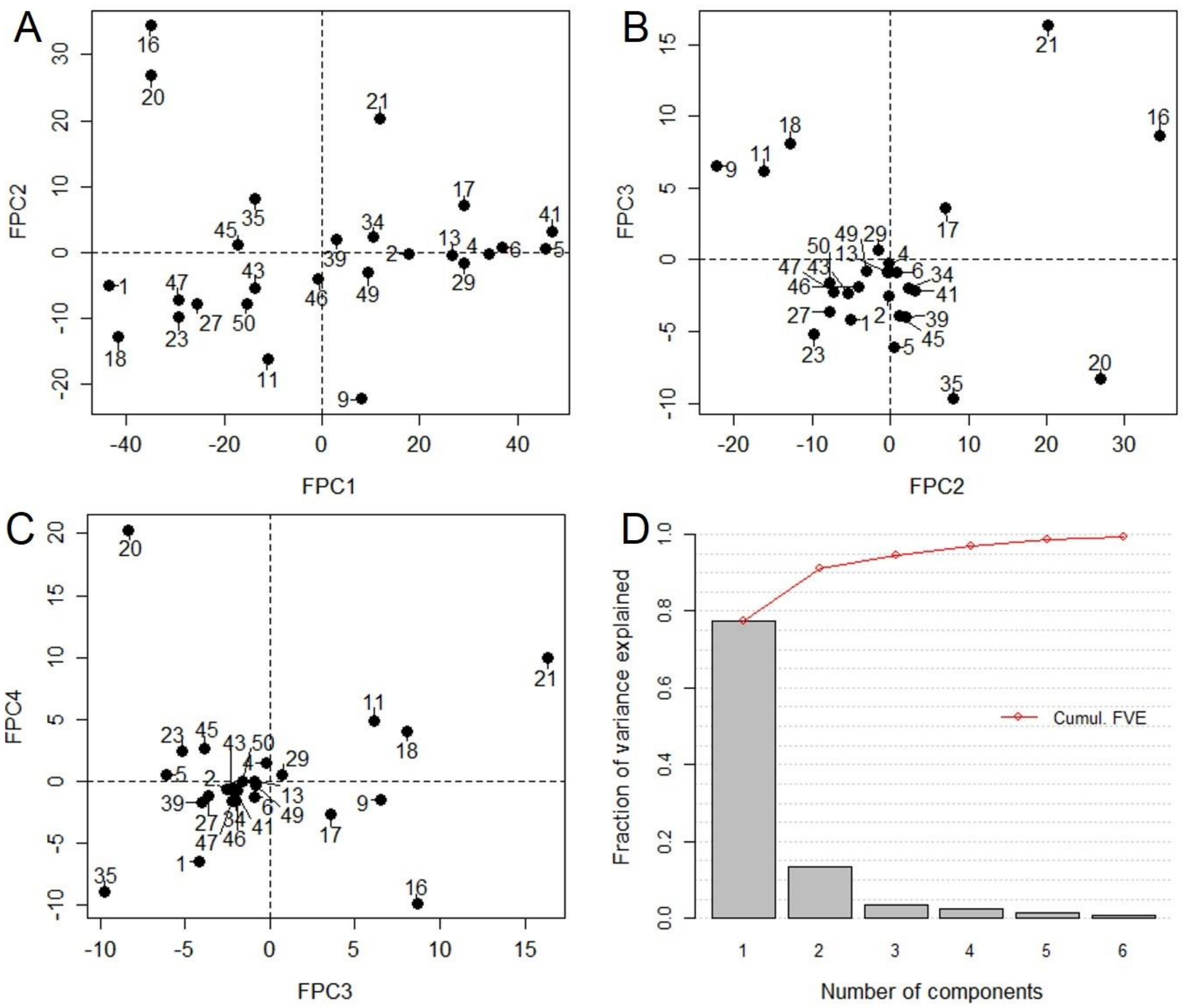

Figure 5: (A) Scatterplot of FPC1 scores compared to FPC2 scores for each drip site. FPC scores reflect the degree of similarity to the respective FPC where zero is more similar. Numbers indicate sites, i.e. 21 is HW_21b. (B) Scatterplot of FPC2 scores compared to FPC3 scores for each drip site (C) Scatterplot of FPC3 scores compared to FPC4 scores for each drip site. Outliers are defined as HW_20b, HW_21b, HW_11b, HW_18b, HW_9b, HW_16b and HW_35b (D) Scree plot displaying fraction of variance explained by each FPC, along with the cumulative variance.

3.4.2. Mean Function and Eigenfunctions

The functional mean derived from FDA (Figure 6A) shows the average curve representative of all loggers across time (Yao et al., 2005). There is less percolation in 2015 compared to 2016, as is expected in the climatic context, with the curve remaining within the bounds of approximately 316 to 3162 drips per day (~ 2.5 to 3.5 when $\log_{10}$ scaled) (Figure 6A). As the mean never reaches zero drips, this provides an indication of a consistent dripping source across most drip sites.

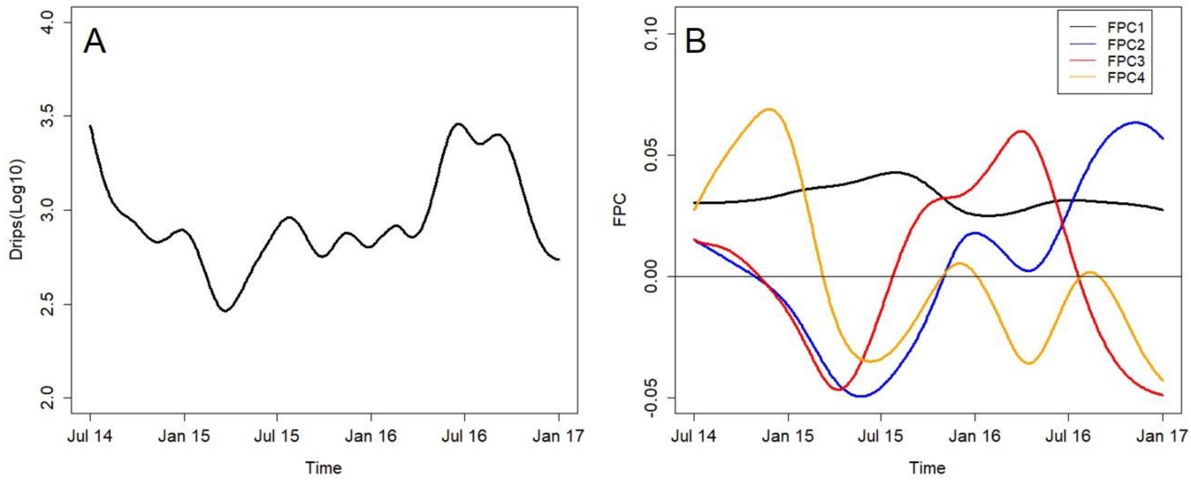

Figure 6: (A) Functional mean of all drip sites over time. An increase in drip rate corresponds with wetter conditions. (B) First four eigenfunctions (FPCs) from FPCA, explaining 97% of the variance.

The estimated eigenfuctions display the major patterns of variation in the drip rate time series and reflect behavioural changes over time (Wang et al., 2016; Yao et al., 2005). Overall, the first four eigenfunctions (FPC1, FPC2, FPC3, FPC4) explained 97% of variations across the drip timeseries (Figure 9D). The first eigenfunction (FPC1) explains 78% of the variance capturing the weighted mean of the sample and is consistently positive and relatively flat, signifying little change in drip variation in the cave over the monitoring period (Figure 6B). This further indicates relatively constant dripping from all loggers, supported by the high fraction of variance explained. A slight peak was recorded in mid 2015, indicating an increase in variability in drip behaviour at that time. The second eigenfunction (FPC2) explained 13% of the variance and reflects two distinct peaks increasing in magnitude over time in January 2016 and January 2017 (Figure 6B). This indicates an annual cyclical pattern that is representative of change in drip water hydrology across the hydrological year. The lowest point recorded for FPC2 corresponds with the peak in FPC1 signalling that the greatest variance across the sample was recorded in winter 2015. The third eigenfunction (FPC3) captures 4% of sample variation and corresponds with the differences in annual patterns of drip behavious (Figure 5B). Finally, the fourth eigenfunction (FPC4) explains only 3% of variation, with the smaller wavelengths indicative of short term or seasonal behaviour of drip water hydrology (Figure 6B). Given these results, the eigenfunctions can be further interpreted to each represent a different mechanism driving drip behaviour, aligned to a specific karst structure. As the first three eigenfunctions represent ~95% of the data, they can be used to indicate three cave water percolation types: storage baseflow, fracture baseflow and overflow as detailed below.

Storage Baseflow (SB): Represented by FPC1, the dominant mode of variation indicating steady, consistent variation of the drip rate time series (Figure 6B). The constant nature of the curve over the monitoring period indicates that drip sites are fed by a storage reservoir that fills and drains over time, establishing a baseflow for relevant drip sites. This group can be further split into SB(a) which are faster dripping (positive FPC1 score) and SB(b) which are slower dripping (negative FPC1 score).

Fracture Baseflow (F) – Represents sites dominated by FPC2 (Figure 6B) which explains changes over the hydrological year, by displaying two obvious increases in percolation over consecutive years (Figure 6B). The increase of percolation in 2016, provides further evidence that this mode of variation is linked to soil moisture and precipitation. Drip rate time series exhibiting this behaviour are likely to have a strong connectivity to the surface through a fracture and be impacted heavily by subsequent percolation events, ensuring a non-constant flow.

Overflow (O) – Characterised by FPC3 that represents sites displaying different behaviour during a drier than average hydrological year and a wetter than average hydrological year. The shift from negative in mid-2015 to highly positive in 2016 is due to increased saturation of the soil and water volume in in any perched water stores (Figure 6B). This can be interpreted as overflow from storage reservoirs that occur as spill over when the reservoir fills to a certain point. The variability of the curve indicates that this behaviour is non-constant.

A summary of drip site hydrological variables, FPC scores and percolation groups are provided in Table 1. As storage baseflow is defined by the dominant mode of variation (Table 1), it explains the most drip sites, followed by smaller groupings exhibiting fracture baseflow and overflow behaviours. Sites classified as SB were further categorised into secondary groups; SB(a) and SB(b) based on whether they were identified as outliers, thus exhibiting behaviour that deviates from the average drip behaviour in Figure 5. It is important to note that generally drip sites display a mix of hydrological behaviours (Arbel et al., 2010; Mahmud et al., 2018), as shown by drip sites recording relatively high FPC scores for multiple eigenfunctions (Figure 5). Therefore, for this categorization, drip sites were grouped by their FPC scores in relation to other drip sites (Figure 5) and not necessarily based on the largest score recorded.

Table 1: Summary of descriptive statistics of each drip site, following a depth profile and indicating section of cave. FPC scores for each eigenfunction are displayed

Logger	Depth (m)	Overburden (m)	Median Daily Drips	Max Daily Drips	FPC1	FPC2	FPC3	FPC4	Percolation group
Cave Entrance									
HW_16b	-7	32	176	25234	-35.02	34.42	8.66	-9.85	F
HW_17b	-7	35	6940	162668	28.92	7.09	3.58	-2.61	SB (a)
Upper Chamber									
HW_46b	-17	49	834	2242	-0.80	-4.02	-1.88	-0.78	SB (b)
HW_6b	-18	55	11577	234710	36.88	0.79	-0.92	-1.31	SB (a)
HW_4b	-19	56	10974	363200	34.10	-0.25	-0.23	1.45	SB (a)
HW_5b	-19	55	31605	202150	45.67	0.55	-6.09	0.56	SB (a)
HW_49b	-20	62	1742	3798	9.45	-3.05	-0.79	-0.32	SB (a)
HW_47b	-20	61	79	133	-29.43	-7.25	-2.21	-1.55	SB (b)
HW_50b	-20	61	269	471	-15.46	-7.72	-1.60	0.03	SB (b)
HW_43b	-21	50	282	523	-13.65	-5.47	-2.31	-0.62	SB (b)
HW_45b	-22	48	338	923	-17.25	1.10	-3.86	2.65	SB(b)
HW_35b	-22	59	216	27503	-13.62	8.12	-9.71	-8.95	O
HW_2b	-22	56	3058	35086	17.65	-0.22	-2.50	-0.65	SB (a)
HW_41b	-23	53	25590	355671	46.92	3.24	-2.13	-0.56	SB (a)
HW_1b	-23	53	14	3697	-43.49	-5.03	-4.17	-6.52	SB (b)
Fracture Zone									
HW_29b	-23	51	7804	15979	29.01	-1.58	0.69	0.50	SB (a)
HW_27b	-23	51	116	204	-25.53	-7.73	-3.65	-1.14	SB (b)
HW_39b	-24	55	1110	6481	2.83	2.06	-3.97	-1.70	SB (a)
Lower Chamber									
HW_13b	-31	61	6875	15101	26.57	-0.36	-0.87	0.01	SB (a)
HW_34b	-31	61	1659	23009	10.48	2.33	-1.96	-1.56	SB (a)
HW_18b	-31	61	40	537	-41.77	-12.86	8.09	3.98	O
HW_9b	-31	62	2455	223392	8.05	-22.21	6.52	-1.46	O
HW_11b	-31	62	529	5633	-11.13	-16.22	6.14	4.91	O
HW_23b	-31	62	104	459	-29.38	-9.88	-5.17	2.43	SB (b)
HW_20b	-31	62	346	241711	-34.84	26.91	-8.33	20.29	F
HW_21b	-31	62	8947	102344	11.72	20.26	16.32	9.94	F

FPC1 and FPC2 explain the majority of variance, therefore corresponding FPC scores for each site are the most meaningful for interpreting general drip dynamics (Figure 5A). Scores close to the x-axis of the FPC1/FPC2 plot have a strong alignment to the average drip behaviour exhibited in the cave. HW_5b, HW_6b and HW_4b have high positive FPC1 scores indicating sites recording greater than average drips at a high frequency. Sites recording a negative FPC1 score record lower than average drips, and also display a larger spread into FPC2 (Figure 5A), indicating a mixture of cave drip dynamics at the lower dripping sites. The clear outliers of the FPC1/FPC2 plot are HW_16b, HW_20b with low FPC1 scores and high FPC2 scores, inferring that the high variability is explained by FPC2.

The outliers are further pronounced in the FPC2/FPC3 plot (Figure 5B), with HW_20b, HW_16b and HW_21b recording high FPC2 scores. HW_9b, HW_11b and HW_18b cluster with low FPC2 scores and relatively high FPC3 scores, displaying similar behaviour in those two dimensions. HW_35b records the lowest FPC3 score, indicating a similar trajectory to the FPC3, but in the opposite direction. FPC3 and FPC4 explain little variability in the context of the whole dataset, but the FPC3/FPC4 plot (Figure 5C) reflects the consistence of the outying FPC scores and respective sites.

4. Discussion

The time series analyses allowed for an understanding of spatiotemporal variability of hydrological response across drip sites. In this section, further consideration is given to interpretation of FPCA to conceptualise a hydrological model, and relevance to existing work.

4.2. Conceptual Model

To further understand similarities and dissimilarities in drip behaviour, the smooth predictive trajectories for each site, derived from FPCA, are grouped using drip percolation type (Figure 7). The storage baseflow group show a large range in total trip volume, but the actual curves for each drip remain within a smaller range with some seasonal fluctuations (Figure 7A). This group of drip sites experiences continuous percolation across wet and dry periods, suggesting that a large homogenised epikarst or soil storage reservoir is feeding drip sites in the upper chamber. Storage baseflow sites are distributed throughout the cave, with nearly all drip sites in the upper chamber displaying this behaviour.

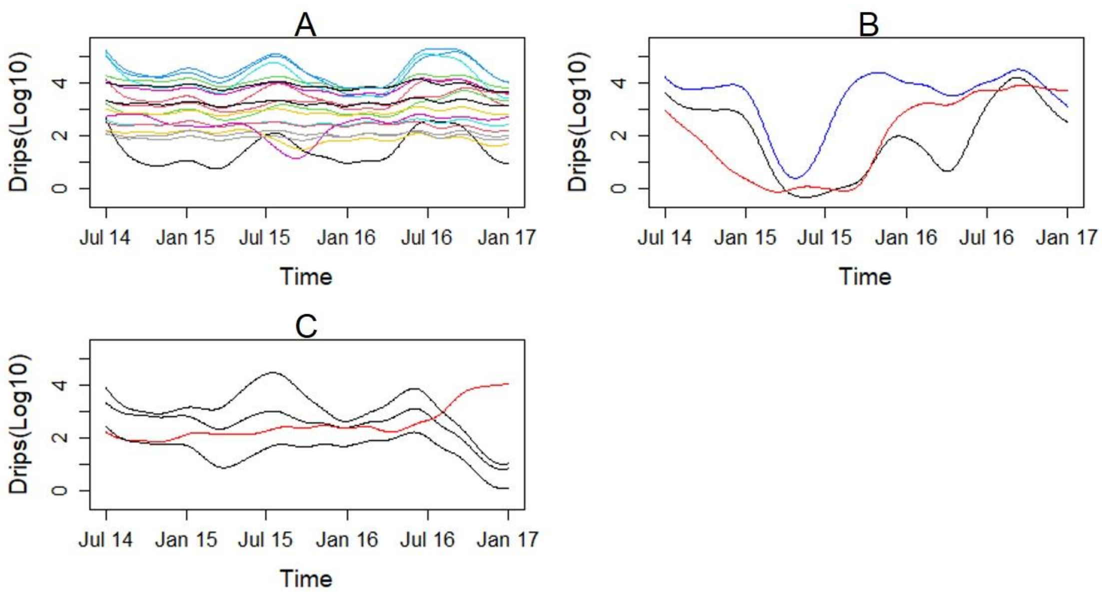

Figure 7: (A) Storage Baseflow group with curves displaying relatively similar trajectories. All curves are relatively flat compared to secondary groups. (B) Fracture baseflow group. HW_16b is the red curve, HW_20b is the black curve and HW_21b is the blue curve. (C) Overflow group with sites in the lower chamber highlighted in black and the upper chamber site (HW_35b) highlighted in red.

In contrast, the drip sites defined by fracture baseflow behaviour display the greatest range across all the sites, reflecting the “flashy” nature of the percolation events (Figure 7B). These sites recorded less dripping in 2015 compared to 2016, showing a clear increase in percolation rate in periods of greater precipitation, although the events were not homogenous across the group (Figure 10B). HW_16b and HW_20b recorded very little drip water activity in winter 2015, with both recording an event in late 2015, albeit at different magnitudes. This implies that fractures feeding these sites “de-activate” in prolonged dry periods and take longer to re-activate if dependent upon prolonged wetting. HW_20b experiences an increase in dripping from May 2015 (Figure 10B), aligning with an increase in precipitation, suggesting this fracture site may have greater connectivity to the surface.

HW_21b and HW_20b are adjacent to each other in the lower chamber, on the southern side of the fracture feature (Figure S2). The fracture feature could be focusing flow and directly feeding these two drip sites. HW_16b is located at the entrance of the cave, under approximately half (32 m) of the overburden compared to the lower chamber. Therefore, it is logical that this drip site has a greater connectivity to the surface, and percolation water is supplied by a fracture.

Drip sites exhibiting overflow behaviour are identified as having relatively low drip rates, until a significant prolonged shift in direction (Figure 7C). HW_9b, HW_11b, HW_18b recorded negative FPC2 scores defining behavioural shift in the opposite direction to FPC2, which infers that these drip sites would be fed by “overflow” when the fracture fed drip sites were dry. These three sites cluster on the FPC2/FPC3 scatter plot (Figure 5B) indicating similar behaviour, with an overflow drainage period observed from July 2016 (Figure 7C). HW_35b differs by increased dripping from July 2016, with positive FPC2 and negative FPC3 values (Figure 7C). This shift to positive values suggests initiation of overflow from July 2016. The temporal difference in overflow behaviour could be explained by drip site location. HW_9b, HW_18b and HW_11b are all situated within ~3m of each other in the lower chamber, on either side of the fracture feature, characterised by two cave shawls with a sharp transition to cave popcorn (Figure S2). This suggests multiple modes of calcite deposition localised in the lower chamber, indicating contrasting flows consistent with the classifications. The cave popcorn indicates a wet environment (Frumkin et al., 2018) with potential for overflow if the epikarst is already relatively saturated. Furthermore, no speleothem growth is present at the overflow drip sites in the lower chamber, as drip feeding is relatively sporadic. HW_35b is in the upper chamber, on the southern side, and could be experiencing overflow from the epikarst storage reservoir for that region.

Using all available information, a conceptual box model can be created to reveal the karst processes feeding drip sites (Figure 8).

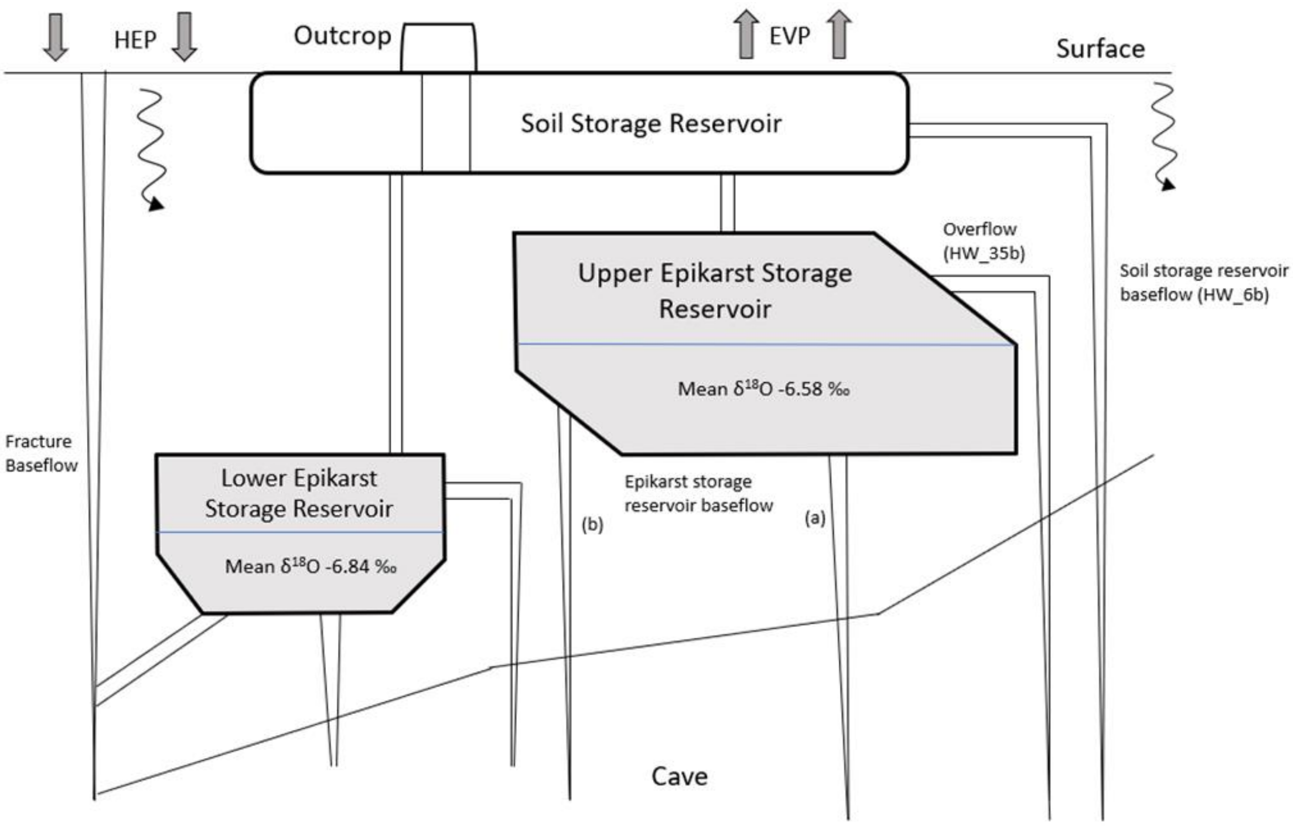

Figure 8: Conceptual box model of cave water percolation routes from the surface to Harrie Wood Cave. Hydrologically effective precipitation (HEP) is the hydroclimatic inputs (precipitation), counteracted by evapotranspiration, mostly from the soil storage reservoir.

Based on the percolation classes for each drip site, the hydrological model demonstrates a hydrological dependence on storage baseflow, particularly in the upper chamber, which suggests the presence of an overarching epikarst storage reservoir. Cross-correlation analysis revealed a strong relationship between soil moisture and percolation rate, especially for HW_6b (Figure 5C), suggesting that the soil storage reservoir is a strong input into the cave hydrology. In March 2015, HW_6b recorded the most positive $\delta^{18}O$ value (-4.32 ‰) which is higher than the Precipitation Weighted Mean (PWM) of 7.0 ‰, and may be indicative of higher evapotranspiration of the soil reservoir due to drier conditions.

Observations of patches of soil on the surface above the cave (Figure S1) do not vertically align with the loggers responding strongly to soil moisture (HW_6b, HW_4b). This suggests that the infiltration into the unsaturated zone from the soil water store occurs preferentially along an axis, potentially the bedding planes. The 3D map of the terrain (Figure S1) also supports the idea of a lack of spatial stationarity of infiltration of water from the soil into the karst.

Drip water percolation into the cave only has a weak relationship with precipitation, indicating a possible hydraulic effect across the epikarst storage reservoir (Coleborn et al., 2016). Previous studies have also found a weak relationship between precipitation and drip discharge during 2011 – 2012 in Harrie Wood Cave (Markowska et al., 2015), and our 2014 – 2017 analyses confirm this indirect influence of precipitation on most sites, indicating the dominant role of the epikarst storage reservoir.

Fracture baseflow sites displayed strong interannual variation in percolation rate, indicating higher reliance on preferential flow through fractures, which may be due to their greater connectivity to the surface. HW_16b's proximity to the entrance, with a smaller overburden, may influence its behaviour, while water at HW_20b and HW_21b may be supplied by perched water flowing from the fracture feature above the lower chamber.

Overflow was identified in both the upper and lower chambers, however the contrasting behaviour of drip sites in each chamber suggests that they may be associated with two distinct epikarst storage reservoirs of different sizes. The stable isotopic spatial heterogeneity, split down the fracture zone (Figure 7), provides further evidence for the presence of two epikarst storage reservoirs. Predicted trajectories (Figure 7C) show that the smaller lower chamber reservoir overflows prior to the larger upper chamber reservoir.

4.3. Comparison with Existing Work

Previous research of Harrie Wood Cave has focused on an analysis of karst hydrology (Markowska et al., 2015) and the implications for interpretations of isotopic signals for paleoclimate reconstruction (Tadros et al., 2022). Drip water from Harrie Wood Cave has also been analysed for stable isotopes and trace elements, with stable isotopic composition from three long-term monitoring drip sites indicating that percolation waters derived from a well-mixed epikarst storage reservoir, with trace and major element composition indicating the role of dilution in wet periods (Tadros et al., 2016). Markowska et al. (2015) identified five drip percolation classes in Harrie Wood Cave, including mixed flow storage connectivity, non-linear, overflow, extreme event activated and underflow. Most of their drip sites aligned with mixed flow storage connectivity, which is similar to the storage baseflow percolation class identified in this study for sites HW_2b, HW_5b, HW_6b and HW_13b. However, there were differences in the classifications of some sites, such as HW_9b, which was classified as non-linear, and HW_11b, which was classified as extreme activated and overflow in the 2012 and 2014-2017 respectively (Markowska et al., 2015). These classifications suggest a threshold must be surpassed before dripping can begin, with a non-linear relationship between drip discharge and precipitation (Baker and Brunsdon, 2003) representative of overflow behaviour. It is important to note that the shorter observation period of Markowska et al. (2015) was dominated by La Niña conditions, which may have influenced the drip behaviour at some sites. For example, it is possible HW_9b and HW_11b were already at saturation point during the observation period, which could have made it difficult to distinguish between different drip classes. This highlights the need to analyse drip behaviour in contrasting hydroclimatic conditions to gain a more comprehensive understanding of the underlying processes.

In this study, we used FPCA to identify persistent modes of variation arising from underlying drip dynamics while accounting for serial autocorrelation. In doing so, the drip percolation classes are reduced to three, simplifying the conceptual model. Additionally, we found that previous analyses by Markowska et al. (2015) were based on drip sites with higher drip rates and higher magnitude than our larger analysis here, potentially skewing identified drip classes. Therefore, it is important to consider spatial and temporal variability in drip behaviour when undertaking these analyses.

4.3.1. Harrie Wood Cave Speleothem Record

A recent study by Tadros et al. (2022) provided insights into the hydrological history of Harrie Wood Cave through a time series analysis of $\delta^{18}O$ variations from three stalagmites dating back to 1922. Despite some short-term discrepancies in $\delta^{18}O$ values between stalagmites, the long-term trend reflected periods of high recharge associated with wetter conditions and low recharge associated with drier conditions. This provides strong evidence that there are sufficiently large epikarst stores in Harrie Wood Cave, with water flow to the cave drip sites every year, even during periods of drought.

Two of the stalagmites used in Tadros et al. (2022) were sourced from the upper chamber ~ 2 m away from HW_1b and HW_41b, whilst the third stalagmite was originally located in the lower chamber, ~ 2m from HW_18b (Figure 2B). The upper chamber stalagmites displayed similarities in hydrochemistry (Tadros et al., 2022), suggesting that they are fed from a common source. As both HW_1b and HW_41b display storage baseflow drip behaviour, it can be deduced that this region is predominantly fed by an epikarst storage reservoir, localised to the upper chamber. In contrast, the stalagmite from the lower chamber recorded a higher offset in $\delta^{18}O$ values (Tadros et al., 2022), indicating that it is supplied by a different hydrological store that is likely smaller than the upper chamber epikarst reservoir.

The stable water isotope sampling from 2014-2016 (Figure 2D) supports this interpretation, with spatial differences in isotopic signature most pronounced surrounding the lower chamber fracture feature, where drip flow regimes are the most variable. Overall, the findings suggest that Harrie Wood Cave has multiple hydrological stores, with distinct water isotopic signatures and drip flow regimes, emphasizing the importance of careful selection and interpretation of drip sites when using stalagmites as a proxy for past climate conditions.

4.4. Hydrological Significance

4.4.1. Implications for speleothem paleoclimate archives

Speleothems are important climate archives, preserving trace element and isotopic information as they grow (McDonough et al., 2022; Treble et al., 2005). However, their reliability as paleoclimate proxies is limited by the complex and variable drip hydrology and karst controls that influence their development. For example, speleothem $\delta^{18}O$ values can widely vary within a single cave due to differences in flow paths (Treble et al., 2022) and isotopic mixing in the soil and epikarst storage zones (Baldini et al., 2006).

This study has implications for speleothem research at both local and global scales. Locally, it supports the hypothesis that the primary hydrological supply to drip sites in Harrie Wood Cave is through storage reservoirs (Markowska et al., 2015; Tadros et al., 2016). The extracted trace elements and water stable isotopes from speleothems in Harrie Wood Cave can thus be interpreted accordingly, given the well mixed nature of the epikarst storage reservoir (Tadros et al., 2019). However, the relatively homogeneous stable water isotope signal may be more useful for decadal trends, rather than specific precipitation events.

The lower chamber of Harrie Wood Cave exhibits the greatest isotopic and hydrologic variability, as well as preferential flow likely associated with the fracture feature. The speleothem from the lower chamber analysed in Tadros et al. (2022) reflected a slightly different signal compared to those from the upper chamber due to the smaller epikarst reservoir (Tadros et al., 2022). Comparison of stalagmites from the lower chamber to those from the upper chamber may help to assess extent of the homogenised stable water isotope signal in Harrie Wood Cave (Tadros et al., 2022). This study provides further understanding of karst controls that affect speleothem development in Harrie Wood Cave and may aid in resolving conflicting palaeo-signals derived from stalagmites in the region (Scroxton et al., 2021).

4.4.2. Implications for cave hydrological monitoring

Conventional approaches to cave drip classification involve analysing discrete drip rate observations to differentiate between timeseries displaying quick flow, including fracture flow, and base flow, incorporating seepage flow (Baker et al., 1997; Smart and Friederich, 1987). However, this approach has been difficult to apply in studies in regions where inter-annual precipitation variability is high or in water limited environments where percolation events are uncommon. This is the case in Southeast Australia (Markowska et al., 2015; McDonald and Drysdale, 2007), due to prolonged changes in water balance due to ENSO fluctuations. By using FPCA, this problem can be addressed as the seasonal signal from the drip data is extracted as a mode of variation. The subsequent weight of this signal is also quantified.

The novel application of FPCA to cave hydrology presented in this study has proved useful to separate karst hydrological controls from surface hydroclimatological inputs. This procedure can be applied to any cave globally, provided there is some form of extended drip monitoring, including drip monitoring data with significant gaps that are not suitable for conventional statistics. The rise of automated drip loggers in recent years has led to a shift from manual methods, leaving some datasets disjointed as a shift in data collection method occurred across monitoring periods (McDonald and Drysdale, 2007). An advantage of FPCA is its ability to utilise drip data derived from any method, serving to effectively link datasets that have different sampling frequencies. Generating long term hydrological datasets with predictive capacities is extremely important in the context of climate change (Klaas et al., 2020) and could allow for baseline data to be established with minimal additional data. Such datasets could be used for research purposes or for broader groundwater management.

Furthermore, FPCA is not limited to drip rate data. There is potential to apply the methods used in this research to drip water stable isotope time series, longer than the $\delta^{18}O$ spot sampling campaign used in this study (Table S1), to analyse stable isotope values over extended time periods. This would provide valuable insights into the inter annual and seasonal mechanisms of drip water percolation, and further support interpretations of isotopic records for paleoclimate reconstruction.

5. Conclusion

This research identifies that the drip water percolation dynamics of Harrie Wood Cave are largely controlled by the epikarst storage reservoirs, which has implications for the water isotopic signals of percolation waters flowing from these features, and the nature of recharge from the unsaturated zone to the underlying aquifer. In addition, our novel application of FDA proves feasibility of this technique in the field of karst hydrology and demonstrates the advantages of considering drip rate time series as a function, which can be utilised for baseline estimations and hydrological projections in both groundwater research and paleoclimate analyses.

The application of FPCA to the drip rate time series revealed three distinct percolation classes: storage baseflow, fracture baseflow and overflow, with secondary classifications occurring within the storage baseflow group. These different percolation classes determine the percolation water drip rate variability, with fracture baseflow having the greatest connectivity to the surface and overflow the least. Regarding the impact of climate, the results indicated that most of the drip rate variation remained relatively low (due to the role of storage baseflow) across years influenced by El Niño and a negative IOD, respectively. However, drip sites in the secondary drip percolation classes displayed greater sensitivity to climate forcings, especially the fracture baseflow group.

In terms of the relationship between drip discharge and environmental factors, positive relationships were found between drip rate, soil moisture, and precipitation, using cross-correlation analysis. Soil moisture had a stronger relationship to drip rates than precipitation, indicating its importance to cave drip water percolation. However, due to the presence of the epikarst storage reservoir, drip rate response to precipitation was muted and relatively constant.

Finally, the spatial distribution of the identified drip classes suggested the importance of a homogenous epikarst storage reservoir. Applying $\delta^{18}O$ variability to drip flow classification inferred the existence of two epikarst storage reservoirs. The lower chamber revealed greater spatial heterogeneity for drip behaviour and corresponding $\delta^{18}O$ values, likely due to a smaller epikarst reservoir and significant fracture feature.

A recommendation for future research would be to apply the methods from this study to identify shifts in cave drip water hydrology time series. Precipitation patterns are changing globally due to climate change, affecting drip water percolation rates into the vadose zone (Barron et al., 2012). FPCA allows for a climatic signal to be extracted from cave drip water percolation time-series and monitored for change. With the continued generation of long drip hydrology time-series (Madmud et al., 2018; Tadros et al., 2022), such analyses would be very useful for understanding how baseflow and hydroclimate inputs have changed over time and to allow for predictions into the future.

Acknowledgements

Thank you to National Parks and Wildlife Service, especially Bernadette Zanet, for allowing access to Harrie Wood Cave and permitting drone use. Thank you to Mira Van Der Ley and Adrian Fisher for pre-flight training and assistance for drone footage collection. Carol Tadros (ANSTO) is thanked for the soil moisture data. Project management and facilitation of data collection by Pauline Treble is greatly appreciated. Katie Coleborn and Tom Cresswell are thanked for their field work assistance. Barbora Gallagher and Jennifer van Holst are also thanked for their assistance in water isotope analyses. Support from the National Centre for Groundwater Research and Training and the NCRIS Groundwater Infrastructure Initiative made this study possible.

Funding

This study was supported by the Australian Research Council Discovery Project DP200100203, and AINSE through a scholarship.

Data availability

Drip time series data is available at: 10.6084/m9.figshare.21516186. R notebooks are available at https://github.com/rebeccachap/Drip-Logger-Time-Series.

References

Aneiros, G., Cao, R., Fraiman, R., Genest, C., Vieu, P., 2019. Recent advances in functional data analysis and high-dimensional statistics. J Multivar Anal 170. https://doi.org/10.1016/j.jmva.2018.11.007

Arbel, Y., Greenbaum, N., Lange, J., Inbar, M., 2010. Infiltration processes and flow rates in developed karst vadose zone using tracers in cave drips. Earth Surf Process Landf 35. https://doi.org/10.1002/esp.2010

Baker, A., Barnes, W.L., Smart, P.L., 1997. Variations in the discharge and organic matter content of stalagmite drip waters in Lower Cave, Bristol. Hydrol Process 11. https://doi.org/10.1002/(SICI)1099-1085(199709)11:11<1541::AID-HYP484>3.0.CO;2-Z

Baker, A., Brunsdon, C., 2003. Non-linearities in drip water hydrology: An example from Stump Cross Caverns, Yorkshire. J Hydrol (Amst) 277. https://doi.org/10.1016/S0022-1694(03)00063-5

Baker, A., Scheller, M., Oriani, F., Mariethoz, G., Hartmann, A., Wang, Z., Cuthbert, M.O., 2021. Quantifying temporal variability and spatial heterogeneity in rainfall recharge thresholds in a montane karst environment. J Hydrol (Amst) 594. https://doi.org/10.1016/j.jhydrol.2021.125965

Baldini, J.U.L., McDermott, F., Fairchild, I.J., 2006. Spatial variability in cave drip water hydrochemistry: Implications for stalagmite paleoclimate records. Chem Geol 235, 390–404. https://doi.org/10.1016/j.chemgeo.2006.08.005

Barron, O. v., Crosbie, R.S., Dawes, W.R., Charles, S.P., Pickett, T., Donn, M.J., 2012. Climatic controls on diffuse groundwater recharge across Australia. Hydrol Earth Syst Sci 16, 4557–4570. https://doi.org/10.5194/hess-16-4557-2012

Brush, J., 2016. Show Caves and Surrounds , in: Ellis, R., Halbert, E. (Eds.), Caves and Karst of Yarrangobilly . Sydney Speleological Society Inc , Sydney , pp. 49–67.

Bureau of Meterology, 2022. Daily Rainfall Yarrangobilly Caves [WWW Document]. Climate Data Online.

Callow, N., McGowan, H., Warren, L., Speirs, J., 2014. Drivers of precipitation stable oxygen isotope variability in an alpine setting, Snowy Mountains, Australia. Journal of Geophysical Research: Atmospheres 119, 3016–3031. https://doi.org/10.1002/2013JD020710

Campbell, M., Callow, J.N., McGrath, G., McGowan, H., 2017. A multimethod approach to inform epikarst drip discharge modelling: Implications for palaeo-climate reconstruction. Hydrol Process 31. https://doi.org/10.1002/hyp.11392

Chen, K., Zhang, X., Petersen, A., Müller, H.-G., 2017. Quantifying Infinite-Dimensional Data: Functional Data Analysis in Action. Stat Biosci 9, 582–604. https://doi.org/10.1007/s12561-015-9137-5

Clements, R., Sodhi, N.S., Schilthuizen, M., Ng, P.K.L., 2006. Limestone karsts of southeast Asia: Imperiled arks of biodiversity. Bioscience. https://doi.org/10.1641/0006-3568(2006)56[733:LKOSAI]2.0.CO;2

Coleborn, K., Rau, G.C., Cuthbert, M.O., Baker, A., Navarre, O., 2016. Solar-forced diurnal regulation of cave drip rates via phreatophyte evapotranspiration. Hydrol Earth Syst Sci 20. https://doi.org/10.5194/hess-20-4439-2016

Cuthbert, M.O., Baker, A., Cuthbert, Jex, C.N., Graham, P.W., Treble, P.C., Anderson, M.S., Acworth, R.I., 2014. Drip water isotopes in semi-arid karst: Implications for speleothem paleoclimatology. Earth Planet. Sci. Lett. https://doi.org/10.1016/j.epsl.2014.03.034

Ellis, S.A., Cobb, K.M., Moerman, J.W., Partin, J.W., Bennett, A.L., Malang, J., Gerstner, H., Tuen, A.A., 2020. Extended Cave Drip Water Time Series Captures the 2015–2016 El Niño in Northern Borneo. Geophys Res Lett 47. https://doi.org/10.1029/2019GL086363

Fairchild, I.J., Baker, A., Asrat, A., Domínguez-Villar, D., Gunn, J., Hartland, A., Lowe, D., 2012. Speleothem Science: From Process to Past Environments, Speleothem Science: From Process to Past Environments. https://doi.org/10.1002/9781444361094

Fairchild, I.J., Tuckwell, G.W., Baker, A., Tooth, A.F., 2006. Modelling of dripwater hydrology and hydrogeochemistry in a weakly karstified aquifer (Bath, UK): Implications for climate change studies. J Hydrol (Amst) 321, 213–231. https://doi.org/10.1016/j.jhydrol.2005.08.002

Ford, D., 2007. Speleogenesis: The development of cave systems, Karst Hydrogeology and Geomorphology.

Ford, D., Williams, P., 2013. Karst Hydrogeology and Geomorphology, Karst Hydrogeology and Geomorphology. https://doi.org/10.1002/9781118684986

Friedrich, H. & Smart, P. L., 1982. The classification of autogenic percolation waters in karst aquifers: A study in G.B. Cave, Medip Hills, England. Proc Univ Bristol Spelaeol Soc 16.

Frumkin, A., Aharon, S., Davidovich, U., Langford, B., Negev, Y., Ullman, M., Vaks, A., Yaʻaran, S., Zissu, B., 2018. Old and recent processes in a warm and humid desert hypogene cave: ʻA’rak Naʻasane, Israel. Int J Speleol 47, 307–321. https://doi.org/10.5038/1827-806X.47.3.2178

Gajardo A, Bhattacharjee S, Carroll C, Chen Y, Dai X, Fan J, Hadjipantelis P, Han K, Ji H, Zhu C, Müller H, Wang J, 2021. fdapace: Functional Data Analysis and Empirical Dynamics.

Genty, D., Deflandre, G., 1998. Drip flow variations under a stalactite of the Pere Noel cave (Belgium). Evidence of seasonal variations and air pressure constraints. J Hydrol (Amst) 211. https://doi.org/10.1016/S0022-1694(98)00235-2

Goldscheider, N., 2019. A holistic approach to groundwater protection and ecosystem services in karst terrains. Carbonates Evaporites 34, 1241–1249. https://doi.org/10.1007/s13146-019-00492-5

Goldscheider, N., Chen, Z., Auler, A.S., Bakalowicz, M., Broda, S., Drew, D., Hartmann, J., Jiang, G., Moosdorf, N., Stevanovic, Z., Veni, G., 2020. Global distribution of carbonate rocks and karst water resources. Hydrogeol J 28, 1661–1677. https://doi.org/10.1007/s10040-020-02139-5

Hael, M.A., 2021. Modeling of rainfall variability using functional principal component method: a case study of Taiz region, Yemen. Model Earth Syst Environ 7. https://doi.org/10.1007/s40808-020-00876-w

Hartmann, J., Jansen, N., Dürr, H.H., Kempe, S., Köhler, P., 2009. Global CO2-consumption by chemical weathering: What is the contribution of highly active weathering regions? Glob Planet Change 69, 185–194. https://doi.org/10.1016/j.gloplacha.2009.07.007

Hassani, S., Martens, H., Qannari, E.M., Kohler, A., 2012. Degrees of freedom estimation in Principal Component Analysis and Consensus Principal Component Analysis. Chemometrics and Intelligent Laboratory Systems 118. https://doi.org/10.1016/j.chemolab.2012.05.015

Jex, C., Mariethoz, G., Baker, A., Graham, P., Andersen, M., Acworth, I., Edwards, N., Azcurra, C., 2012. Spatially dense drip hydrological monitoring and infiltration behaviour at the Wellington Caves, South East Australia. Int J Speleol 41, 283–296. https://doi.org/10.5038/1827-806X.41.2.14

Jung, P.H., Song, J., 2021. Multivariate Neighborhood Trajectory Analysis: An Exploration of the Functional Data Analysis Approach. Geogr Anal. https://doi.org/10.1111/gean.12298

Kempe, S., 1979. Carbon in the rock cycle. SCOPE 13. The global carbon cycle.

Klaas, D.K.S.Y., Imteaz, M.A., Sudiayem, I., Klaas, E.M.E., Klaas, E.C.M., 2020. Assessing climate changes impacts on tropical karst catchment: Implications on groundwater resource sustainability and management strategies. J Hydrol (Amst) 582, 124426. https://doi.org/10.1016/j.jhydrol.2019.124426

Mahmud, K., Mariethoz, G., Baker, A., Treble, P.C., 2018. Hydrological characterization of cave drip waters in a porous limestone: Golgotha Cave, Western Australia. Hydrol Earth Syst Sci 22. https://doi.org/10.5194/hess-22-977-2018

Markowska, M., Baker, A., Treble, P.C., Andersen, M.S., Hankin, S., Jex, C.N., Tadros, C. v., Roach, R., 2015. Unsaturated zone hydrology and cave drip discharge water response: Implications for speleothem paleoclimate record variability. J Hydrol (Amst) 529. https://doi.org/10.1016/j.jhydrol.2014.12.044

Markowska, M., Cuthbert, M.O., Baker, A., Treble, P.C., Andersen, M.S., Adler, L., Griffiths, A., Frisia, S., 2020. Modern speleothem oxygen isotope hydroclimate records in water-limited SE Australia. Geochim Cosmochim Acta 270. https://doi.org/10.1016/j.gca.2019.12.007

McDonald, J., Drysdale, R., 2007. Hydrology of cave drip waters at varying bedrock depths from a karst system in southeastern Australia. Hydrol Process 21. https://doi.org/10.1002/hyp.6356

McDonough, L.K., Treble, P.C., Baker, A., Borsato, A., Frisia, S., Nagra, G., Coleborn, K., Gagan, M.K., Zhao, J. xin, Paterson, D., 2022. Past fires and post-fire impacts reconstructed from a southwest Australian stalagmite. Geochim Cosmochim Acta 325. https://doi.org/10.1016/j.gca.2022.03.020

Nicholl, O., 1974. Harrie Wood Cave Map - Y26. Yarrangobilly Research Group and Canberra Speleological Society.

Partin, J.W., Jenson, J.W., Banner, J.L., Quinn, T.M., Taylor, F.W., Sinclair, D., Hardt, B., Lander, M.A., Bell, T., Miklavic, B., Jocson, J.M.U., Taboroši, D., 2012. Relationship between modern rainfall variability, cave dripwater, and stalagmite geochemistry in Guam, USA. Geochemistry, Geophysics, Geosystems 13. https://doi.org/10.1029/2011GC003930

Peel, M.C., Finlayson, B.L., McMahon, T.A., 2007. Updated world map of the Köppen-Geiger climate classification. Hydrol Earth Syst Sci 11. https://doi.org/10.5194/hess-11-1633-2007

Poulain, A., Watlet, A., Kaufmann, O., van Camp, M., Jourde, H., Mazzilli, N., Rochez, G., Deleu, R., Quinif, Y., Hallet, V., 2018. Assessment of groundwater recharge processes through karst vadose zone by cave percolation monitoring. Hydrol Process 32. https://doi.org/10.1002/hyp.13138

Pracný, P., Faimon, J., Sracek, O., Kabelka, L., Hebelka, J., 2016. Anomalous drip in the Punkva caves (Moravian Karst): Relevant implications for paleoclimatic proxies. Hydrol Process 30. https://doi.org/10.1002/hyp.10731

R Core Team, 2022. R: A Language and Environment for Statistical Computing.

Ramsay, J., Silverman, B., 2005. Functional Data Analysis , 2nd ed. Springer, New York.

Ramsay, J.O., Wang, X., Flanagan, R., 1995. A Functional Data Analysis of the Pinch Force of Human Fingers. Appl Stat 44. https://doi.org/10.2307/2986192

Rangata, M., Das, S., Ali, M., 2020. Analysing maximum monthly temperatures in South Africa for 45 years using functional data analysis. Advances in Decision Sciences 24. https://doi.org/10.47654/v24y2020i3p1-27

Reinfelds, I., Swanson, E., Cohen, T., Larsen, J., Nolan, A., 2014. Hydrospatial assessment of streamflow yields and effects of climate change: Snowy Mountains, Australia. J Hydrol (Amst) 512, 206–220. https://doi.org/10.1016/j.jhydrol.2014.02.038

Risbey, J.S., Pook, M.J., McIntosh, P.C., Wheeler, M.C., Hendon, H.H., 2009. On the remote drivers of rainfall variability in Australia. Mon Weather Rev 137. https://doi.org/10.1175/2009MWR2861.1

Sari, W.J., Wigena, A.H., Djuraidah, A., 2017. Quantile regression with functional principal component in statistical downscaling to predict extreme rainfall. Int J Ecol Econ Stat 38.

Scroxton, N., Walczak, M., Markowska, M., Zhao, J.X., Fallon, S., 2021. Historical droughts in Southeast Australia recorded in a New South Wales stalagmite. Holocene 31. https://doi.org/10.1177/0959683620981717

Sheffer, N.A., Cohen, M., Morin, E., Grodek, T., Gimburg, A., Magal, E., Gvirtzman, H., Nied, M., Isele, D., Frumkin, A., 2011. Integrated cave drip monitoring for epikarst recharge estimation in a dry Mediterranean area, Sif Cave, Israel. Hydrol Process 25, 2837–2845. https://doi.org/10.1002/hyp.8046

Smart, P.L., Friederich, H., 1987. Water movement and storage in the unsaturated zone of a maturely karstified carbonate aquifer, Mendip Hills, England, in: Proceedings of the Environmental Problems in Karst Terranes and Their Solutions Conference.

Spate, A.G.J., 2016. Geology, Geomorphology and Hydrology of Yarrangobilly , in: Ellis, R., Halbert, E. (Eds.), Caves and Karst of Yarrangobilly . Sydney Speleological Society Inc , Sydney , pp. 75–89.

Stevanović, Z., 2019. Karst waters in potable water supply: a global scale overview. Environ Earth Sci 78, 662. https://doi.org/10.1007/s12665-019-8670-9

Tadros, C. v., Markowska, M., Treble, P.C., Baker, A., Frisia, S., Adler, L., Drysdale, R.N., 2022. Recharge variability in Australia's southeast alpine region derived from cave monitoring and modern stalagmite δ18O records. Quat Sci Rev 295, 107742. https://doi.org/10.1016/j.quascirev.2022.107742

Tadros, C. v., Treble, P.C., Baker, A., Fairchild, I., Hankin, S., Roach, R., Markowska, M., McDonald, J., 2016. ENSO - cave drip water hydrochemical relationship: A 7-year dataset from south-eastern Australia. Hydrol Earth Syst Sci 20. https://doi.org/10.5194/hess-20-4625-2016

Tadros, C. v., Treble, P.C., Baker, A., Hankin, S., Roach, R., 2019. Cave drip water solutes in south-eastern Australia: Constraining sources, sinks and processes. Science of the Total Environment 651. https://doi.org/10.1016/j.scitotenv.2018.10.035

Tagne, G. v., Dowling, C., 2018. Inferring groundwater flow and recharge from time series analysis of storm responses in a karst aquifer of southeastern Kentucky (USA). Hydrogeol J 26, 2649–2668. https://doi.org/10.1007/s10040-018-1837-8

Ternynck, C., Alaya, M.A. ben, Chebana, F., Dabo-Niang, S., Ouarda, T.B.M.J., 2016. Streamflow hydrograph classification using functional data analysis. J Hydrometeorol 17. https://doi.org/10.1175/JHM-D-14-0200.1

Treble, P.C., Baker, A., Abram, N.J., Hellstrom, J.C., Crawford, J., Gagan, M.K., Borsato, A., Griffiths, A.D., Bajo, P., Markowska, M., Priestley, S.C., Hankin, S., Paterson, D., 2022. Ubiquitous karst hydrological control on speleothem oxygen isotope variability in a global study. Commun Earth Environ 3. https://doi.org/10.1038/s43247-022-00347-3

Treble, P.C., Bradley, C., Wood, A., Baker, A., Jex, C.N., Fairchild, I.J., Gagan, M.K., Cowley, J., Azcurra, C., 2013. An isotopic and modelling study of flow paths and storage in Quaternary calcarenite, SW Australia: Implications for speleothem paleoclimate records. Quat Sci Rev 64. https://doi.org/10.1016/j.quascirev.2012.12.015

Treble, P.C., Chappell, J., Gagan, M.K., McKeegan, K.D., Harrison, T.M., 2005. In situ measurement of seasonal δ18O variations and analysis of isotopic trends in a modern speleothem from southwest Australia. Earth Planet Sci Lett 233. https://doi.org/10.1016/j.epsl.2005.02.013

Ullah, S., Finch, C.F., 2013. Applications of functional data analysis: A systematic review. BMC Med Res Methodol 13, 43. https://doi.org/10.1186/1471-2288-13-43

Veress, M., 2020. Karst Types and Their Karstification. Journal of Earth Science 31. https://doi.org/10.1007/s12583-020-1306-x

Wagner-Muns, I.M., Guardiola, I.G., Samaranayke, V.A., Kayani, W.I., 2018. A Functional Data Analysis Approach to Traffic Volume Forecasting. IEEE Transactions on Intelligent Transportation Systems 19. https://doi.org/10.1109/TITS.2017.2706143

Wang, J.-L., Chiou, J.-M., Müller, H.-G., 2016. Functional Data Analysis. Annu Rev Stat Appl 3, 257–295. https://doi.org/10.1146/annurev-statistics-041715-033624

Williams, P.W., 1983. The role of the subcutaneous zone in karst hydrology. J Hydrol (Amst) 61. https://doi.org/10.1016/0022-1694(83)90234-2

Worbys, G., 1982. Kosciuosko National Park Geology and Geomorphology. National Parks and Wildlife Services, Sydney.

Yao, F., Müller, H.G., Wang, J.L., 2005. Functional data analysis for sparse longitudinal data. J Am Stat Assoc 100, 577–590. https://doi.org/10.1198/016214504000001745

Zamprogno, B., Reisen, V.A., Bondon, P., Aranda Cotta, H.H., Reis, N.C., 2020. Principal component analysis with autocorrelated data. J Stat Comput Simul 90. https://doi.org/10.1080/00949655.2020.1764556

Zhou, X., Müller, H.-G., 2022. The dynamics of ideology drift among U.S. Supreme Court justices: A functional data analysis. PLoS One 17, e0269598. https://doi.org/10.1371/journal.pone.0269598

Supplementary Material

Spatiotemporal Variation in Cave Percolation Waters: A Functional Approach

Rebecca G. Chapman[1*], Shawn Laffan[1], Liza K. McDonough[2], Monika Markowska[3], Andy Baker[1]

[1] School of Biological, Earth and Environmental Sciences, UNSW Sydney, NSW, 2052, Australia

[2] Australian Nuclear Science and Technology Organisation (ANSTO), New Illawarra Rd, Lucas Heights, NSW, 2234, Australia

[3] Climate Geochemistry Department, Max Planck Institute for Chemistry, Mainz, 55128, Germany

*Corresponding author: Rebecca.chapman@unswalumni.com

Table S1: $\delta^{18}O$ values for drip water collected at each site. The spot sampling period is from 2014-2016, covering most of the monitoring period. Note: "n.a." indicates where a value is unavailable.

	Mar 14		Jul 14		Jan/Feb 15		Mar 15		Nov 15		Feb 16	
Site (HW_)	$\delta^{18}O$ ‰	2 SE	$\delta^{18}O$ ‰	2 SE	$\delta^{18}O$ ‰	2 SE	$\delta^{18}O$ ‰	2 SE	$\delta^{18}O$ ‰	2 SE	$\delta^{18}O$ ‰	2 SE
1b	n.a.	n.a.	-6.39	0.02	-6.04	0.03	n.a.	n.a.	n.a.	n.a.	n.a.	n.a.
2b	-6.75	0.02	-7.09	0.02	-6.66	0.01	-6.77	0.01	-6.92	0.06	-6.8	0.02
4b	-6.8	0.02	-7.02	0.02	-6.71	0.02	-6.75	0.05	-6.81	0.03	-6.86	0.03
5b	-6.81	0.03	-7.12	0.02	-6.55	0.02	-6.66	0.06	-6.81	0.04	-6.78	0.03
6b	-6.78	0.02	-6.93	0.02	-6.06	0.02	-4.32	0.06	-6.75	0.06	-6.66	0.02
9b	-6.25	0.01	-7.23	0.03	-5.94	0.02	-6.27	0.06	-6.81	0.05	-6.63	0.04
11b	-6.54	0.02	-6.78	0.01	-6.72	0.02	-6.76	0.02	-6.81	0.04	-6.8	0.04
13b	-6.86	0.01	-7.21	0.03	-6.29	0.02	n.a.	n.a.	-6.92	0.05	n.a.	n.a.
16b	-6.86	0.02	-6.99	0.04	n.a.	n.a.	-6.78	0.02	-6.89	0.06	-6.84	0.06
17b	-6.8	0.02	-7.21	0.02	n.a.	n.a.	n.a.	n.a.	-6.87	0.05	-6.89	0.04
18b	-6.42	0.01	-7.19	0.03	n.a.	n.a.	n.a.	n.a.	n.a.	n.a.	n.a.	n.a.
20b	-6.79	0.02	-7.28	0.03	n.a.	n.a.	-6.09	0.02	-6.87	0.07	-6.67	0.02
21b	-6.9	0.03	-7.3	0.02	n.a.	n.a.	n.a.	n.a.	-6.87	0.06	-6.67	0.01
23b	-6.36	0.02	-6.85	0.01	n.a.	n.a.	-6.44	0.20	n.a.	n.a.	-6.58	0.04
27b	-7.03	0.01	-7.01	0.02	n.a.	n.a.	-6.72	0.30	n.a.	n.a.	n.a.	n.a.
29b	-7.2	0.02	-7.22	0.03	n.a.	n.a.	-7.08	0.25	-7.21	0.04	-7.24	0.01
34b	-6.84	0.02	-7.17	0.01	n.a.	n.a.	-6.45	0.02	-6.9	0.08	-6.67	0.04
35b	n.a.	n.a.	-6.71	0.02	n.a.	n.a.	n.a.	n.a.	n.a.	n.a.	-6.73	0.02
39b	-7.22	0.04	-7.26	0.03	-7.18	0.05	-7.09	0.01	-7.23	0.08	-7.15	0.03
41b	-6.97	0.04	-6.91	0.04	-6.97	0.05	-6.81	0.03	-6.95	0.06	-7.01	0.04
43b	-5.97	0.02	-6.64	0.02	-6.74	0.01	-6.51	0.03	n.a.	n.a.	n.a.	n.a.
45b	-6.72	0.02	-6.91	0.01	-6.75	0.03	-6.56	0.03	n.a.	n.a.	-6.93	0.06
46b	-6.55	0.04	-6.85	0.03	-6.69	0.03	n.a.	n.a.	-6.84	0.06	-6.8	0.05
47b	n.a.	n.a.	-6.28	0.02	-6.31	0.01	-5.69	0.01	n.a.	n.a.	n.a.	n.a.
49b	n.a.	n.a.	-6.78	0.02	-6.85	0.01	-6.71	0.02	-5.77	0.06	-6.86	0.02
50b	n.a.	n.a.	-6.38	0.02	-6.41	0.04	-5.98	0.05	n.a.	n.a.	-6.31	0.02

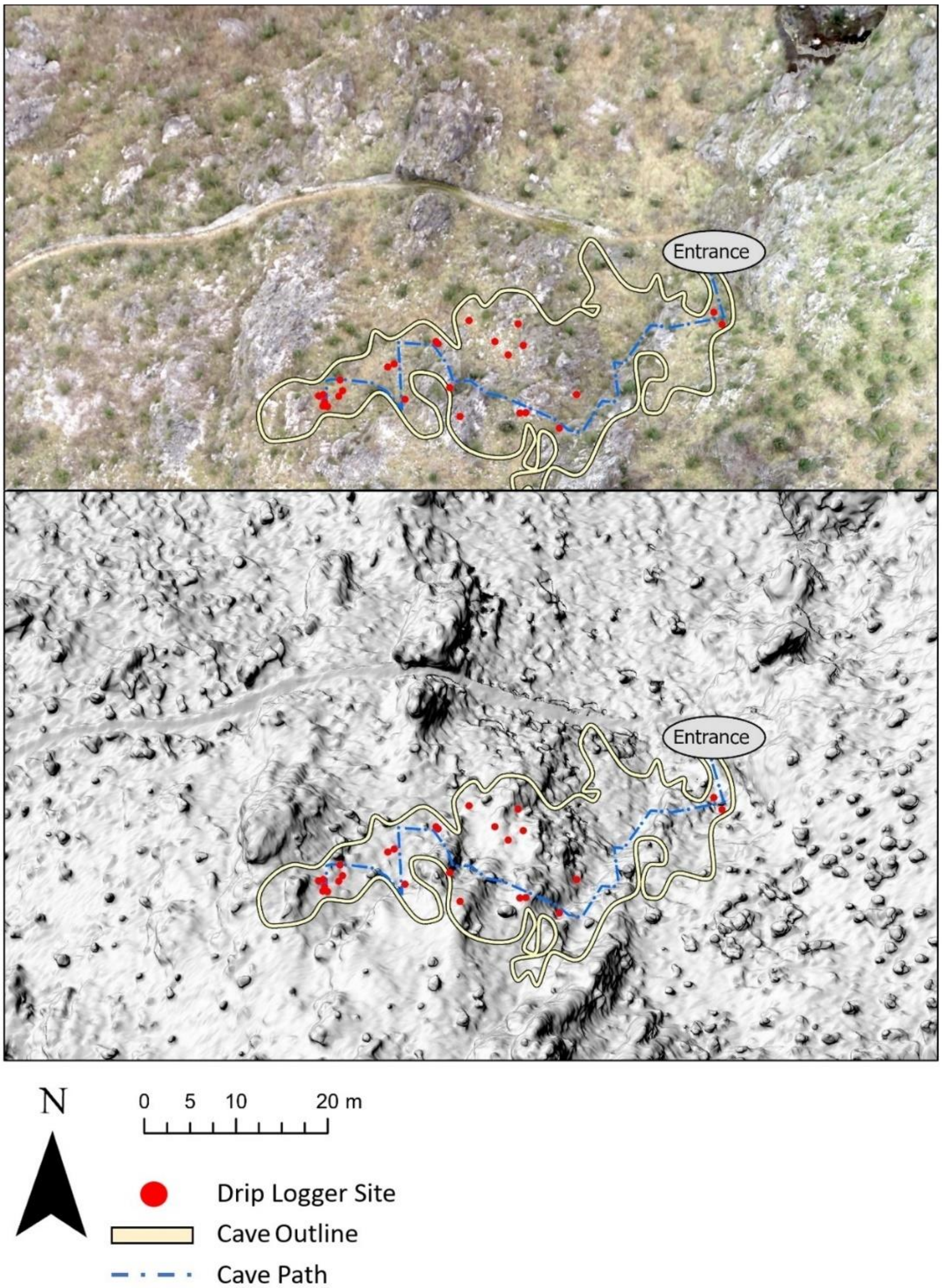

Figure S1**:** (A) Orthomosaic map of the surface of Harrie Wood Cave, with the cave outline overlayed. The red points are location of loggers, and dashed line is the path. Limestone outcroppings are present with minimal vegetation coverage. (B) 3D representation of the surface of Harrie Wood cave generated using ArcGIS Pro 3.0. Geological features are highlighted, to show the irregularities of the cave surface, with NE bedding planes outlined in the exposed rock. Aerial images were collected using a DJI Phantom 4pro drone and Pix4D software (https://www.pix4d.com/). Images were captured with an 80% overlap and converted to a digital surface model (DSM) and orthomosaic using Pix4D Mapper software.

Figure S2: Images from the lower chamber of the cave. This section of cave underlies a fracture zone (upper right). This fracture is represented by a shift from dark limestone to pale limestone. The fracture feature is characterised by cave shawls surrounded by cave popcorn. Fluvial deposits indicative of past phreatic processes are found in this lower chamber.

Figure S3: Images from the upper chamber of the cave, showing that this section of cave contains well developed speleothems and relatively dry conditions.

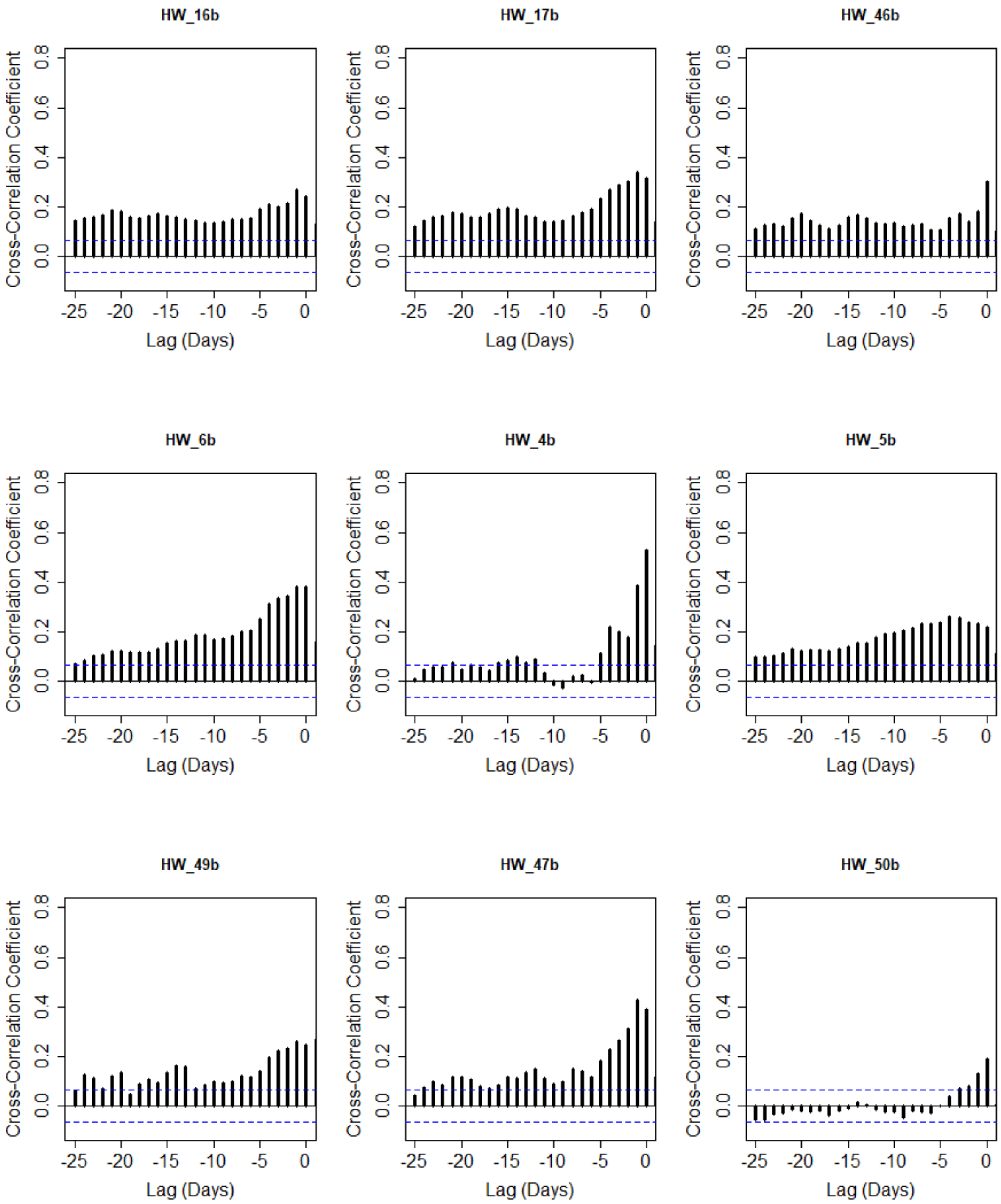

Figure S4: Cross correlation plots of rainfall to drip discharge for each site (labelled). Continued on the next page. The blue dashed line represented the 95% confidence interval for each site.

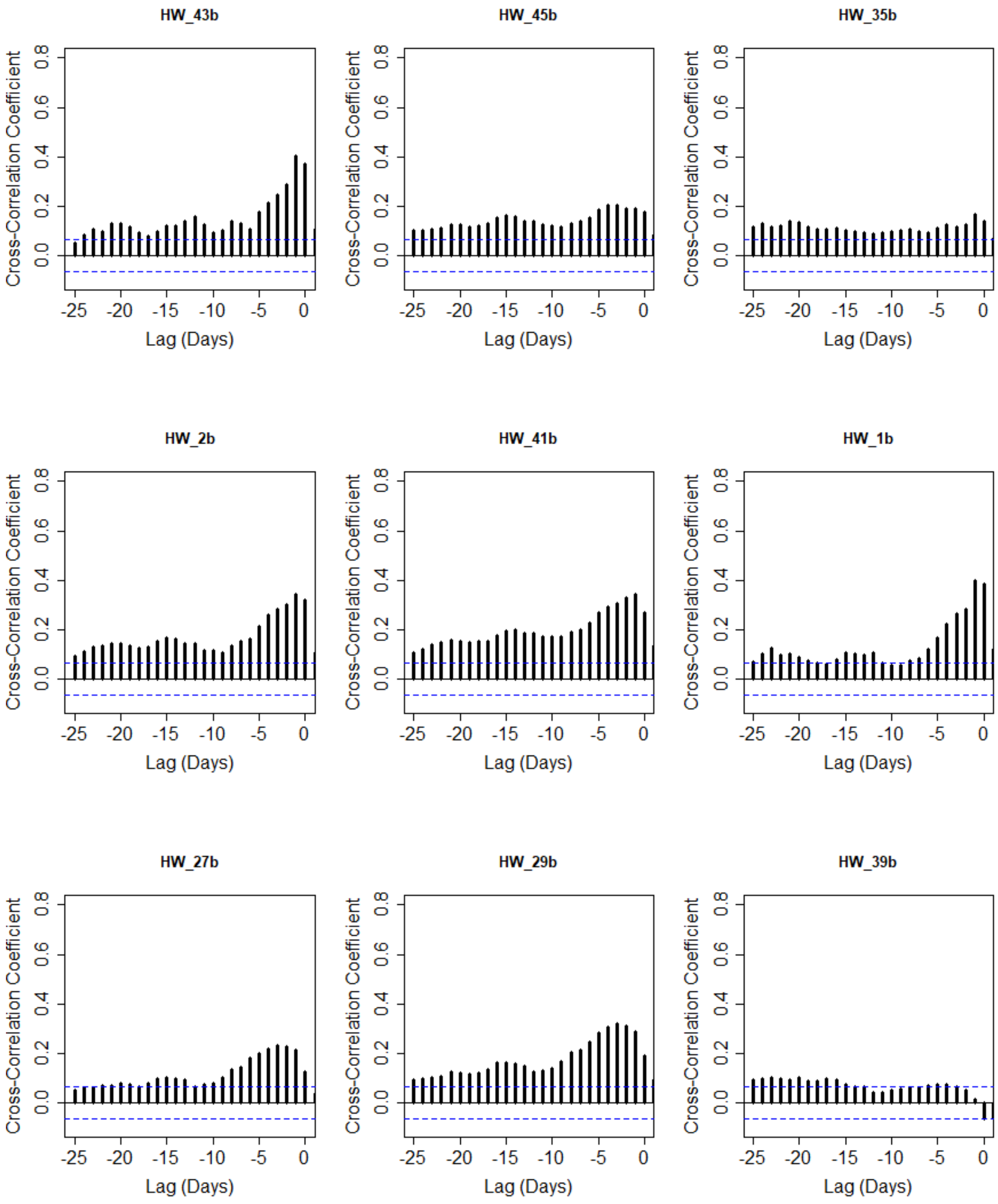

Figure S4 continued: Cross correlation plots of rainfall to drip discharge for each site (labelled)

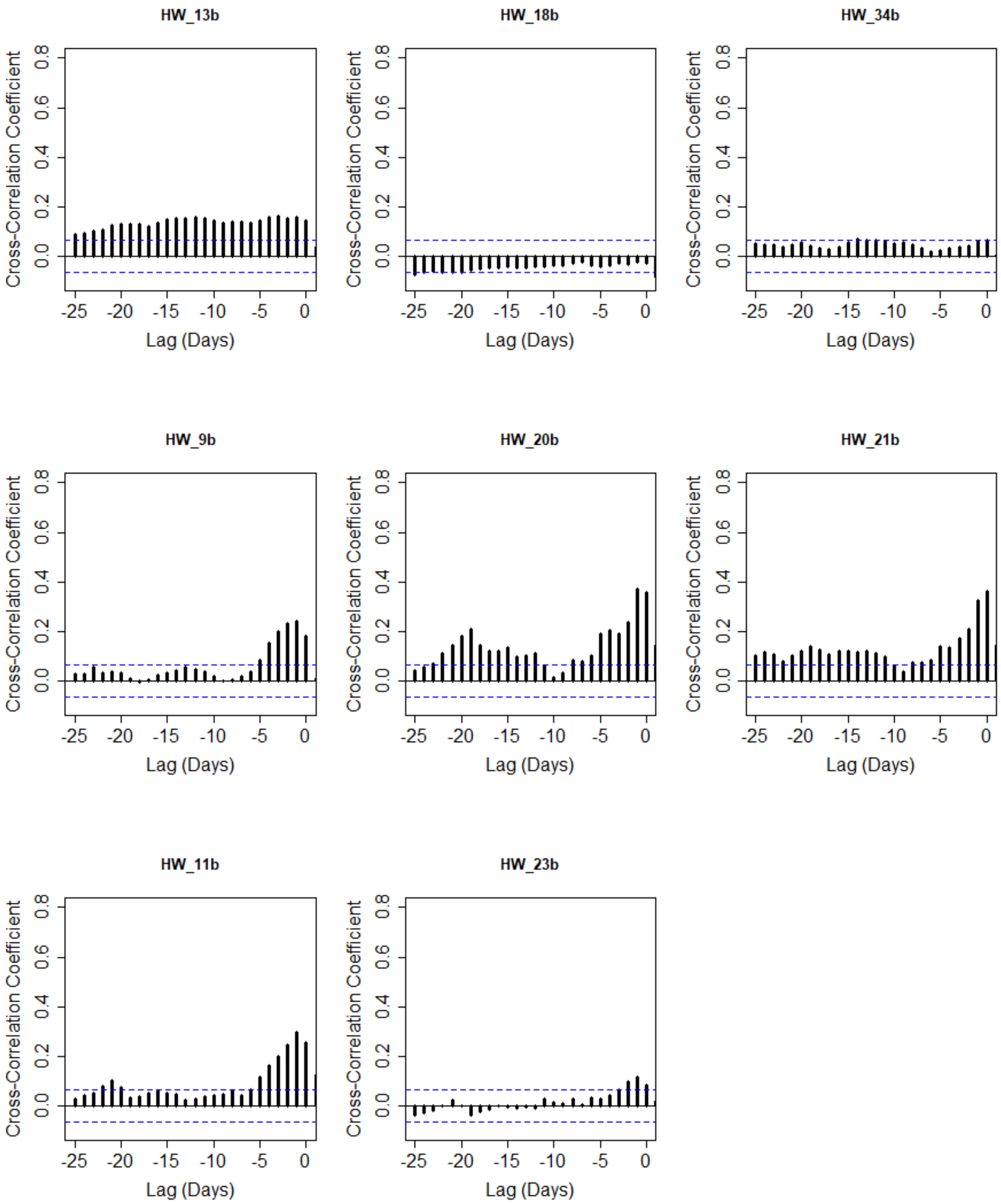

Figure S4 continued: Cross correlation plots of rainfall to drip discharge for each site (labelled)

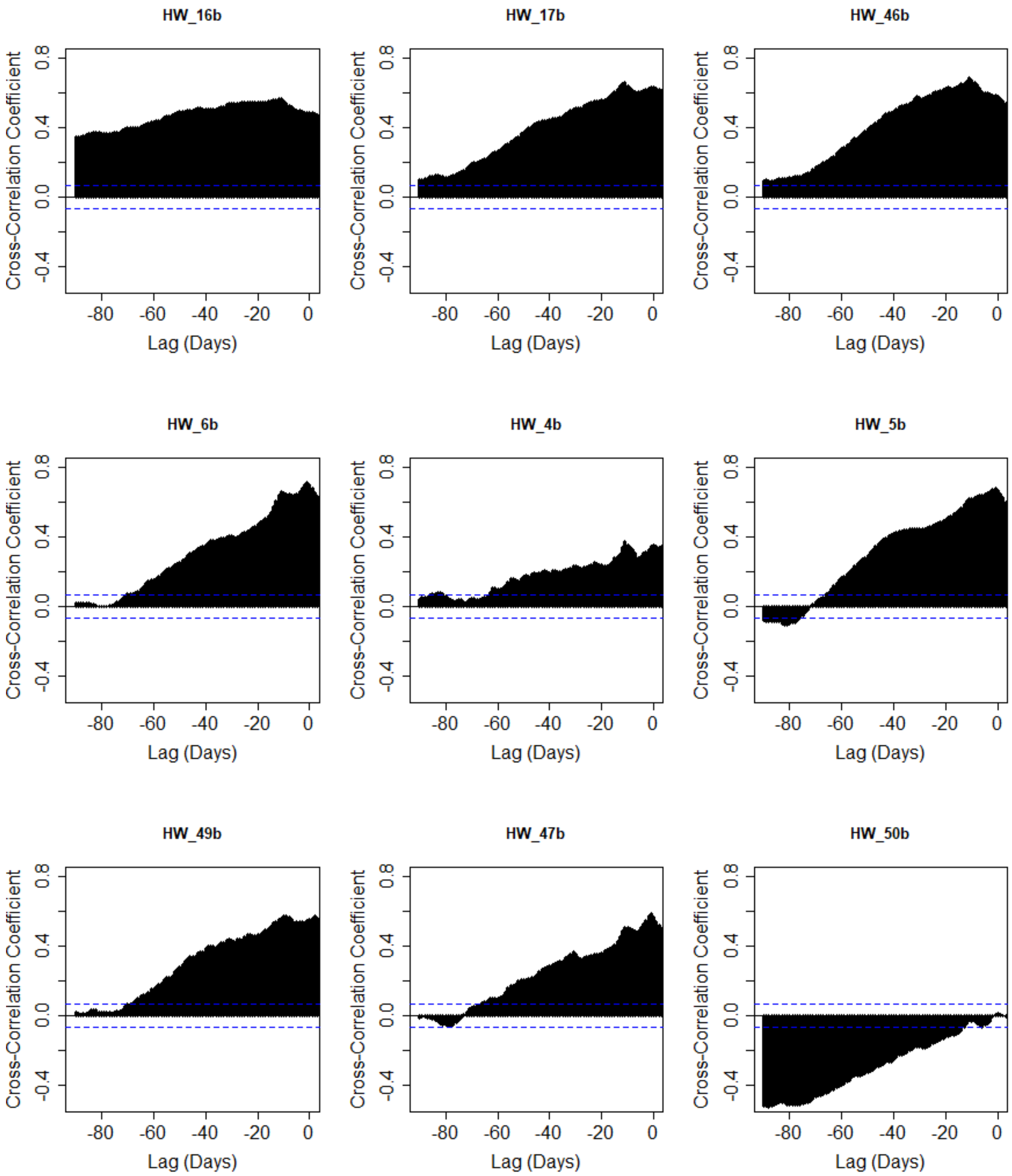

Figure S5: Cross correlation plots of soil moisture to drip discharge for each site (labelled) at a lag of 90 days. The blue dashed line represents the 95% confidence interval for each site. Continued on next page.

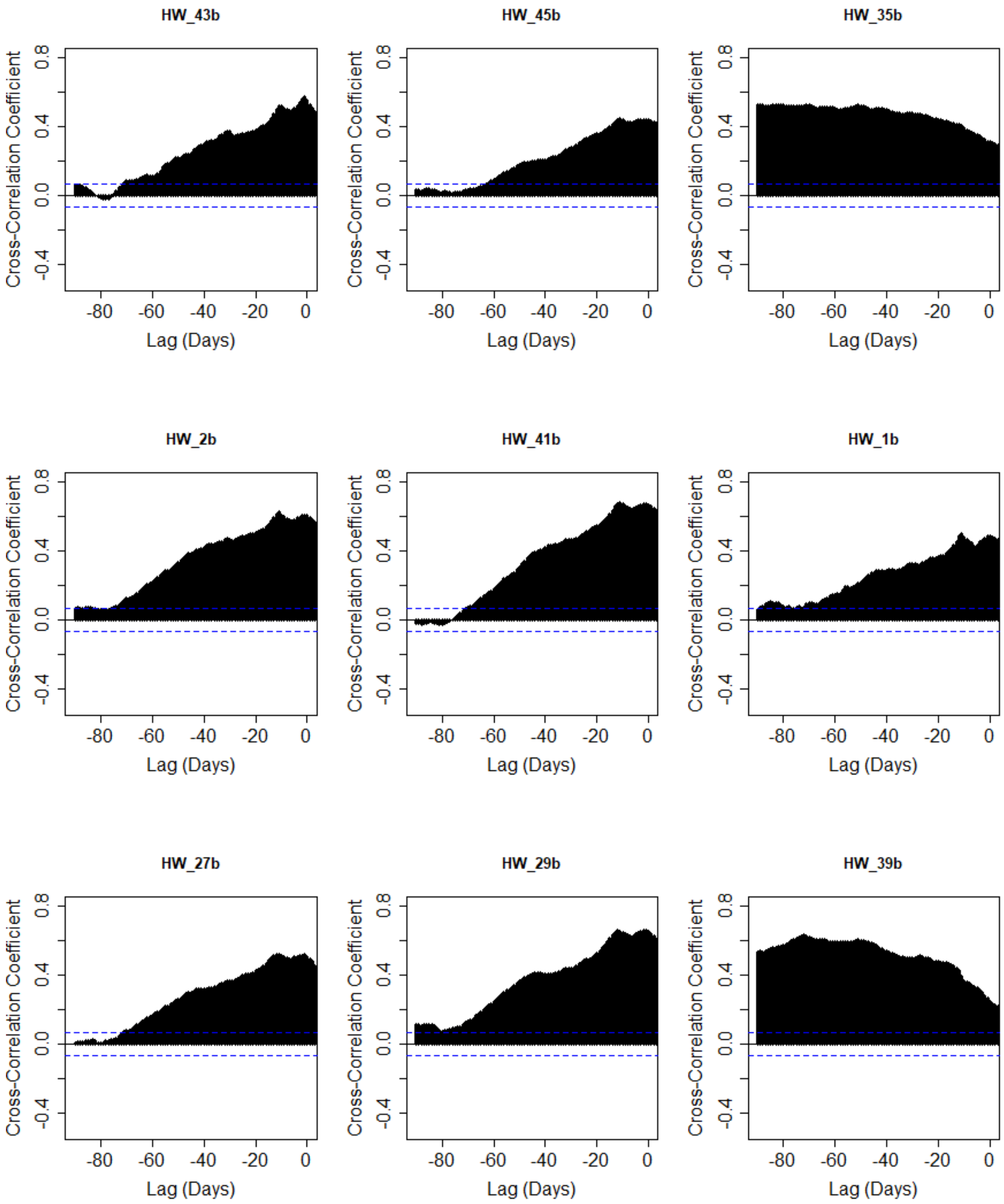

Figure S5 continued: Cross correlation plots of soil moisture to drip discharge for each site (labelled)

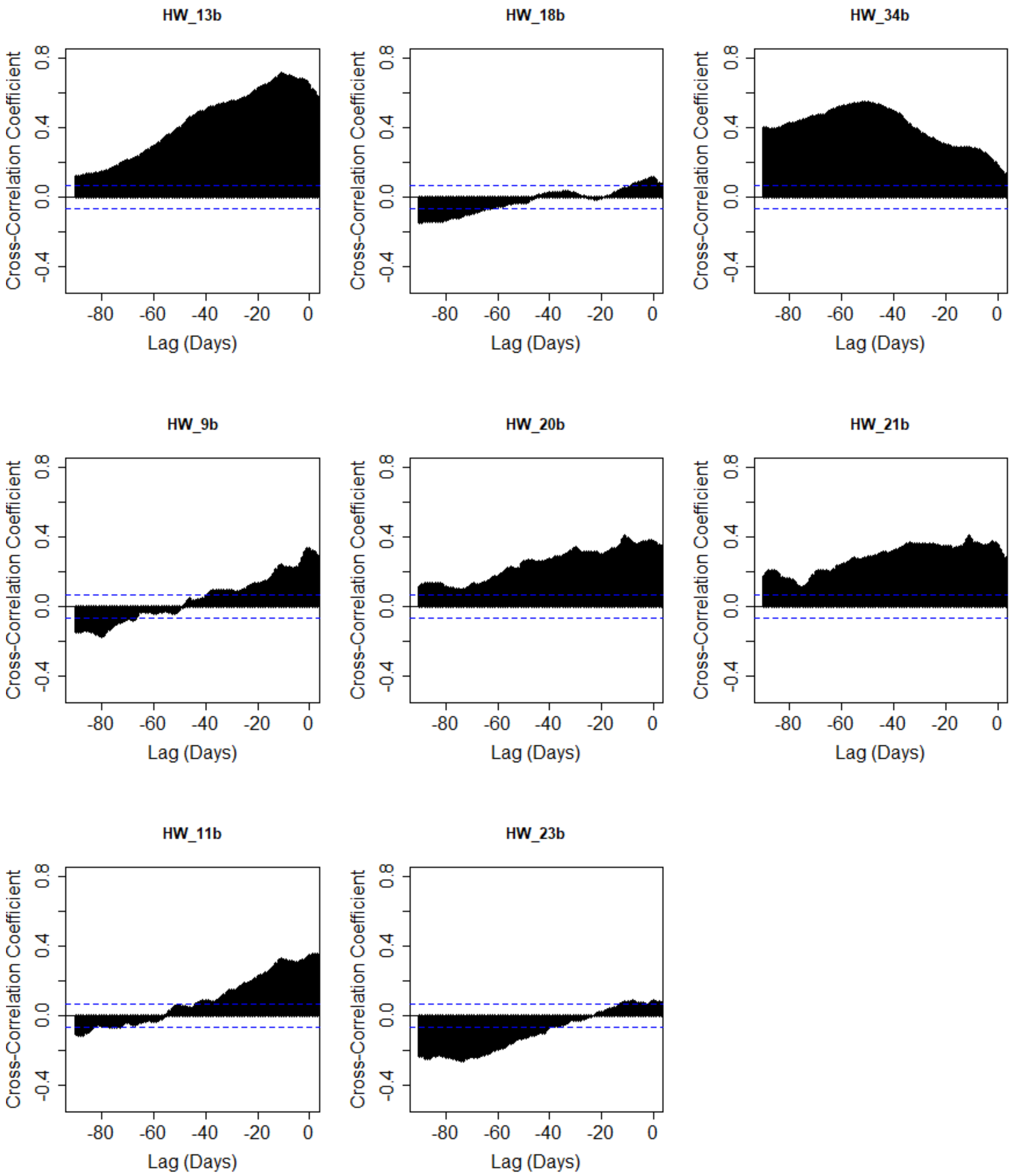

Figure S5 continued: Cross correlation plots of soil moisture to drip discharge for each site (labelled)